Uppsala University

Characterization of dye-sensitized solar cells

Components for environmentally friendly photovoltaics

Hanna Ellis

UPPSALA
UNIVERSITET

Dissertation for the Licentiate of Philosophy in Physical Chemistry

Abstract
As fossil fuels, the major source of energy used today, create the greenhouse gas carbon dioxide which causes global warming, alternative energy sources are necessary in the future. There is a need for different types of renewable energy sources such as hydropower, windpower, wavepower and photovoltaics since different parts of the world have different possibilities. The sun is a never ending energy source. Photovoltaics use the energy of the sun and converts it into electricity. There are different types of photovoltaics and a combination of them could provide humankind with energy in a sustainable way. In this thesis dye-sensitized solar cells are investigated. Materials for the counter electrode have been investigated and resulting in a polymer based cathode outperforming the traditionally used platinized counter electrode in a cobalt-based redox mediator system (paper I). The sensitizer of the TiO_2 was investigated, in this study by modifications of the π-linker unit in an organic donor-linker-acceptor based dye. Four new dyes were synthesized, all four showing extended absorption spectra compared to the reference dye. However, it was found that increasing the absorption spectrum does not necessarily increase the power conversion efficiency of the solar cell (paper II). In the last part of this thesis, water-based electrolyte dye-sensitized solar cells were investigated. A hydrophilic dye with glycolic chains close to the center of regeneration was synthesized. The results show increased wettability by water-based electrolyte for the sensitized surface, increased regeneration and performance for the hydrophilic dye compared to a hydrophobic dye (paper III). The glycolic chains complex with small cations such as Na^+ and K^+ in the electrolyte, this probably facilitate the regeneration of the hydrophilic dye even further (paper IV). In this thesis new materials for a more environmentally friendly dye-sensitized solar cell are investigated.

List of papers

This thesis is based on the following papers, which are referred to in the text by their Roman numerals.

I Hanna Ellis, Nikolaos Vlachopoulos, Leif Häggman, Christian Perruchot, Mohamed Jouini, Gerrit Boschloo, Anders Hagfeldt
PEDOT counter electrodes for dye-sensitized solar cells prepared by aqueous micellar electrodeposition
Electrochimica Acta 107:45–51, 2013

II Hanna Ellis, Susanna Kaufmann Eriksson, Sandra Feldt, Erik Gabrielsson, Peter Lohse, Rebecka Lindblad, Licheng Sun, Håkan Rensmo, Gerrit Boschloo, Anders Hagfeldt
Linker unit modification of triphenylamine-based organic dyes for efficient cobalt mediated dye-sensitized solar cells
The Journal of Physical Chemistry C 117(41):21029–21036, 2013

III Valentina Leandri, Hanna Ellis, Erik Gabrielsson, Licheng Sun, Gerrit Boschloo, Anders Hagfeldt
Organic hydrophilic dye for water-based dye-sensitized solar cells
Physical Chemistry Chemical Physics, DOI: 10.1039/c4cp02774d, 2014

IV Hanna Ellis, Valentina Leandri, Gerrit Boschloo, Anders Hagfeldt, Jonas Bergström, Denys Shevchenko
Laser desorption/ionization mass spectrometry of dye-sensitized solar cells: identification of the dye-electrolyte interaction
Submitted to Journal of the American Society for Mass Spectrometry 2014

Comments on my own contribution

I was the main responsible for paper I and II for which I carried out most of the experimental work, data analysis and writing of the manuscript. In paper III my participation included planning, experimental work and discussion. However, I did not participate in all experimental work and was not the main responsible for the writing of the manuscript. In paper IV I initiated the study and prepared samples. The

MALDI-MS measurements were performed by co-workers and I was not the main responsible for writing the manuscript. I did not perform any synthesis of dyes, redox couples, PES measurements or SEM measurements.

I am a co-author of the following paper which is not included in this thesis.

- Erik Gabrielsson, Hanna Ellis, Sandra Feldt, Haining Tian, Gerrit Boschloo, Anders Hagfeldt, Licheng Sun
  Convergent/Divergent synthesis of a linker-varied series of dyes for dye-sensitized solar cells based on the D35 Donor
  Advanced Energy Materials 3(12):1647–1656, 2013

Contents

Abbreviations

Symbols

$E^{0'}$
: Formal redox potential

E^{0}
: Standard potential

E_{0-0}
: Gap between ground state level and first excited level

E_{CB}
: Energy of conduction band

$E_{F,0}$
: Fermi level in dark conditions

E_{F,TiO_2}
: *quasi*-Fermi level in TiO_2

$E_{F,redox}$
: Redox potential of redox couple

E_F
: *quasi*-Fermi level

E_{bin}
: Binding energy

E_c
: Energy of conduction band edge

E_{kin}
: Kinetic energy of photoelectrons

E_{ox}
: Oxidation peak potential

E_{redox}
: Redox potential

E_{red}
: Reduction peak potential

I_0
: Reference intensity

J_{lim}
: Limiting current density

J_{max}
: Current density at maximum power point

J_{sc}
: Current density at short circuit conditions

N_c
: Effective density of conduction band electrons

ε
: Molar extinction coefficient

η
: Solar cell efficiency

η_{cc}
: Charge collection efficiency

η_{reg}
: Regeneration efficiency

λ
: Inelastic mean free path

ν
: Frequency

ω_d
: Peak frequency

ϕ
: Working function

ϕ_{inj}
: Quantum yield of injected electrons

σ
: Spacing between electrodes

i_{lim}
: Limiting current

k_B
: Boltzman constant

A

A
: Absorbance

a
: area

AC
: Alternating current

AM
: Air mass density

C

C
: Concentration

CDCA
: Chenodyoxylic acid

CE
: Counter electrode

CH_3CN
: Acetonitrile

D
D
: Diffusion coefficient

DSC
: Dye-sensitized solar cell

E
E_f
: Equilibrium Fermi level

EDOT
: 3,4-ethylenedioxythiophene

F
F
: Faraday constant

FF
: Fill factor

FT-IR
: Fourier transform infrared spectroscopy

FTO
: Fluorine doped tin oxide

H
h
: Planck constant

HOMO
: Highest occupied molecular orbital

I
I
: Intensity

I
: Current

IMFP
: Inelastic mean free path

IPCE
: Incident photon to current conversion efficiency

IR
: Infra-red

J
J
: Current density

L

L

Length

LHE

Light harvesting efficiency

LUMO

Lowest unoccupied molecular orbital

M

MALDI-MS

Matrix assisted laser desorption ionization mass spectroscopy

MPN

3-methoxypropionitrile

N

n

Number of electrons

$\mathbf{n}_c$

Density of conduction band electrons

NHE

Normal hydrogen electrode

P

$\mathbf{P}_{in}$

Power of incident light

$\mathbf{P}_{max}$

Maximum power point

PEDOT

Poly(3,4-ethylenedioxythiophene)

PEG

Polyethylene glycol

PES

Photoelectron spectroscopy

PIA

Photoinduced absorption spectroscopy

PMMI

1-propyl-3-methylimidazolium iodide

Q

Q

Extracted charge

q

Elementary charge of an electron

R

R
: Gas constant

r
: Radius

R_{ce}
: Charge transfer resistance at the counter electrode

R_D
: Diffusion resistance

R_{rec}
: Recombination resistance

R_s
: Series resistance

R_{tot}
: Total resistance in the solar cell

S

SEM
: Scanning electron microscopy

T

T
: Transmittance

T
: Temperature

TAS
: Transient absorption spectroscopy

TBP
: 4-tert-butylpyridine

TiO_2
: Titanium dioxide

U

UV
: Ultra violet

V

V
: Voltage

V_{max}
: Voltage at maximum power point

V_{oc}
: Voltage at open circuit conditions

W

WE
: Working electrode

Z
Z
: Impedance

1. Introduction

1.1 Energy demand and energy consumption

The reason why there is research about dye-sensitized solar cells (DSC) and other alternative energy sources is the global warming due to the combustion of fossil fuels. The human society uses extensive resources of energy and a majority of this energy is coming from fossil fuels. The usage of different energy sources for 2013 is illustrated in Figure 1.1.

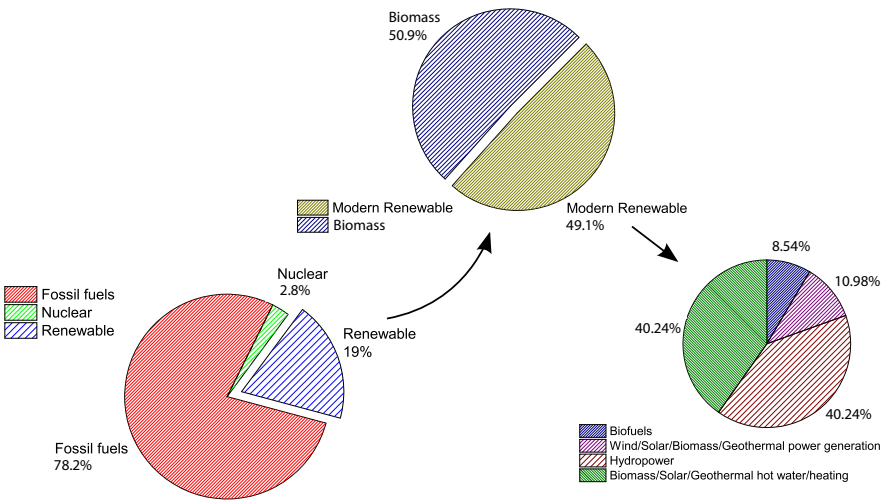

Figure 1.1. Global energy consumption in 2013 [1].

Combustion of fossil fuels creates carbon dioxide (CO_2). Gasoline which is used for many combustion engines contains hydrocarbons of 5 to 12 carbon atoms length. When combusting these hydrocarbons, such as octane, CO_2 is created according to:

$$2\,C_8H_{18} + 25\,O_2 \rightarrow 16\,CO_2 + 18\,H_2O \tag{1.1}$$

CO_2 is a greenhouse gas, which implies that it absorbs and emits IR-radiation. In short; the greenhouse effect is caused by the sun irradiating photons of UV-vis energy onto the earth. The UV-vis light is absorbed on the earth by land mass and sea, and as a result the earth heats up and re-irradiate IR-photons which should exit the atmosphere and leave the earth. The combustion of fossil fuels has lead to anthropogenic emission of carbon dioxide, methane and

other greenhouse gases which has increased the concentration of these gases in the atmosphere. In the atmosphere the greenhouse gases absorb IR-radiation and re-emit it back to the earth, causing global warming of the earth.

Today there is consensus on global warming due to anthropogenic activity. The United Nations Intergovernmental Panel on Climate Change (IPCC) have concluded [2]:

The global average combined land and ocean surface temperature show a warming of 0.85 °C over the period 1880 to 2012. The rate of sea level rise has been larger since the mid-19th century than the mean rate during the previous two millennia. Over the period 1901 to 2010 global mean sea level rose by 0.19 m. Atmospheric concentrations of carbon dioxide, methane, and nitrous oxide have increased to levels unprecedented in at least the last 800,000 years. Carbon dioxide concentrations have increased by 40% since pre-industrial times, primarily from fossil fuel emissions and secondarily from net land use change emissions. The ocean has absorbed about 30% of the emitted anthropogenic carbon dioxide, causing ocean acidification.

The production, investment and usage of renewable energy is growing world wide. Photovoltaics has a huge potential since the sun is a never ending energy source providing us with more energy in an hour than the world human population consumes in a year [3]. There will not be one solution for the renewable energy production in the future. Different regions in the world have different resources. However, a variety of different renewable energy sources, amongst them photovoltaics could make a great contribution, would make the transition from fossil fuels to renewable energy possible.

1.2 Photovoltaics

Photovoltaics (PV) is the collective name for devices converting the energy of the sun, photons, into electricity. The photovoltaic effect refers to when photons are falling upon a semiconductor and generating an electron-hole pair. The electron and the hole can be directed to two different contacts, a circuit can connect the two and an electric potential difference will be established. The photoelectric effect was discovered by Edmond Becquerel in 1839. As this thesis is about dye-sensitized solar cells, it should be mentioned that Becquerel's experiments were performed on liquid photoelectrochemical devices. Becquerel illuminated solutions containing metal halide salts and observed current between two platinum electrodes immersed into the electrolyte. In Figure 1.2 the working principle of a silicon solar cells is illustrated. Two layers, one n-doped and one p-doped are brought together. Upon irradiation the electrons in the n-doped layer move to the excited state, which is the conduc-

tion band. The electrons move in the circuit and arrive at the p-doped layer, after the circuit. The electrons will then move to the n-type layer again due to the energy levels. The process can start again.

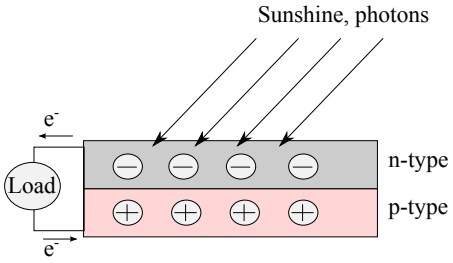

Figure 1.2. Schematic illustration of a silicon solar cell.

There are different kinds of photovoltaics; the traditional silicon solar cells, thin film technologies, organic solar cells, quantum dot solar cells, perovskite solar cells, dye-sensitized solar cells et cetera. Just as renewable energy should be a variety of energy sources in the future, photovoltaics should be a variety of different techniques, since different techniques are advantageous in different situations. Down below follows a brief introduction to different kinds of solar cells (the DSC is introduced in Chapter 2).

Silicon solar cells

Crystalline silicon (Si) photovoltaics is the most widely used photovoltaic technology today. Silicon is the second most abundant element in the earth's crust, however silicon rarely appears as the pure element. Instead it appears as silicon dioxide (silica) or silicates. The advantage of silicon solar cells is the abundance of silicon. The disadvantage is the energy consumption for producing pure silicon. There are two types of crystalline silicon solar cells: mono-crystalline silicon produced by slicing wafers from a high-purity single crystal ingot and multi-crystalline silicon, made by sawing a cast block of silicon first into bars and then into wafers. The mono-crystalline silicon solar cells have higher efficiencies than the multi-crystalline. The record efficiencies of crystalline silicon solar cells are about 25% [4]. The silicon solar cells work with the principle shown in Figure 1.2. Two semiconductors, both silicon, one n-doped (most often with phosphorous) and the other one p-doped (for example with boron) are brought together.

Thin film technologies

Thin film technology devices include amorphous Si, CdS, CdTe, $CuInSe_2$ (CIS) and $CuInGaSe_2$ (CIGS). Thin film technologies solar cells work with the same principle as the crystalline silicon photovoltaics, semiconductors are brought together and an electric field is established at the junction between the

p-type and the n-type inorganic semiconductors. Efficiencies of around 20% have been established for thin film technologies [4].

Organic solar cells
Organic solar cells consist of conductive polymers or other organic conductors as charge transport materials. An analogue to semiconductor based solar cells can be made. Different conductive polymers with different HOMO-LUMO levels are brought together, charge separation is established by effective fields that bring electrons to fall from one excited state level to another. Efficiencies of about 11% have been achieved with organic solar cells [4].

Quantum dot solar cells
There are different types of quantum dot solar cells and they are more or less similar to dye-sensitized solar cells. The quantum dots can be used both as sensitizer and redox mediator and the quantum dot solar cells can be both liquid and solid state based. An example of material for the quantum dots is lead-sulfide. Quantum dot solar cells have attained an efficiency of 8.6% [4].

Perovskite solar cells
Perovskite solar cells are a relatively new technology of photovoltaics. Perovskites encompass a broad class of crystalline minerals. In the perovskite solar cells the kinetics and working principle are still under investigation. The perovskite seems to work both as charge carrier and absorbing material. A disadvantage of the perovskite solar cells is that the record-breaking ones contain lead and that perovskites, being salt-like minerals, readily dissolve in water or even humid air. There is research going on to replace the lead with for example tin and efficiencies of 6.4% have been reported [5]. For the lead version the record efficiency is 17.9% [4].

The Shockley-Queisser limit
Within the photovoltaic field the Shockley-Queisser limit is a maximum theoretical efficiency that solar cells building on the principle of a p-n junction can achieve. The Shockley-Queisser limit was first calculated by William Shockley and Hans Queisser in 1961 [6]. There are a number of processes limiting the efficiency, one of the most important is the limitation of absorption of photons. The band gap of silicon, used for solar cells, is 1.1 eV. As a consequence, the photons from the sun with less energy cannot contribute to the efficiency of the solar cell. In Figure 1.3 the solar irradiance spectrum for AM 1.5 is shown. The band gap of crystalline silicon 1.1 eV, equal to 1127 nm, is indicated.

Another limitation is photons having more energy than the band gap, exciting electrons to higher energy levels and holes to lower levels in the atoms/molecules. Before transport in the semiconductor, the electrons relax down to the lowest energy level (bottom) of the conduction band and the holes move up to the

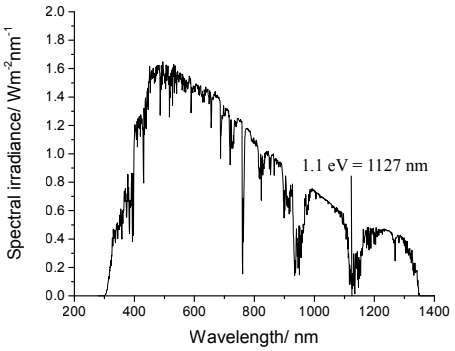

Figure 1.3. Solar irradiance on the surface of the earth, the spectrum illustrate the AM 1.5 irradiance.

valence band ground state level of the semiconductor. This process is called thermalization of hot electrons. The energy difference is lost and this energy cannot contribute to the efficiency of the solar cell. The Shockley-Queisser limit maximizes the efficiency of a single p-n junction solar cell with a band gap of 1.1 eV, using AM 1.5 solar spectrum to about 30% [6]. The efficiency of a combustion engine used in cars running on gasoline is around 30%. The systems are though very different, but the reference is given here in order to point out that the systems, existing commercially today, do not have higher efficiencies.

Generations of photovoltaics

Photovoltaic technologies are divided into three different generations. The first generation of photovoltaics is limited by the Shockley-Queisser limit and the high cost per generated power. Conventional crystalline silicon solar cells belong to the first generation since they demand a lot of energy for the purification of silicon.

Photovoltaic systems belonging to the second generation are still limited by the Shockley-Queisser limit, but this generation provides a lower cost per generated power due to cheaper fabrication process. The thin film technologies belong to the second generation of photovoltaics.

In the third generation of photovoltaics the devices can exceed the Shockley-Queisser limit. Multi-junction (tandem) solar cells and other emerging technologies being able to use hot electrons (higher vibrational energy than ground state) and up-conversion (combining two lower energy photons to one higher) belong to this generation. The third generation of photovoltaics also builds on cheap materials such as nanomaterials and cheap processes where extreme temperatures, such as for producing pure silicon, are not necessary.

This thesis is about dye-sensitized solar cells which could belong both to the second and the third generation of photovoltaics, since they are made of cheap materials and can be considered being constructed as a multi-junction system. The multi-junction is motivated by the semiconductor band gap and the dye HOMO-LUMO gap.

2. Dye-sensitized solar cells - working principles

The basic research leading to the dye-sensitized solar cell (DSC) was done during the 1970-80 [7, 8, 9]. A breakthrough came in 1991 when Grätzel and O'Regan introduced the mesoporous structure of the semiconductor, which gave a significant energy conversion improvement to 7.9% [10]. The mesoporous structure increased the light harvesting due to the increased surface area. Before this breakthrough compact layers of the semiconductor had been used with conversion efficiencies around 1%. With the breakthrough in 1991 a whole research field emerged. Today there are different related solar cell techniques such as solid state DSC [11], quantum dot solar cells [12, 13], p-type DSC [14] and perovskite solar cells [15, 16, 17, 18]. Perovskite solar cells has become a hot topic in the the field since the breakthrough in 2012. There are also a number of alternatives to the liquid electrolyte in DSC such as gel electrolytes, ionic liquids and in-situ polymerized hole conductors [19, 20, 21, 22, 23].

A standard liquid DSC is shown in Figure 2.1. The components of a DSC are: two conductive glass electrodes, usually coated with fluorine doped tin oxide (FTO-glass). One of the electrodes is the anode, the working electrode (WE), which is screen printed with TiO_2 nanoparticles (particle size around 20-50 nm). The TiO_2 is sensitized with a dye, which absorbs the photons. The other electrode is the cathode, the counter electrode (CE) and in between the two electrodes is the electrolyte containing the redox couple.

In Figure 2.1 the different processes in a DSC are shown:

1. The photon is absorbed by the dye and the dye is excited.
2. The electron is injected into the semiconductor.
3. The electron is extracted on the backside of the electrode and goes through the circuit where it can perform electrical work.
4. At the counter electrode the electron reduces the oxidized species of the redox couple in the electrolyte.
5. The reduced species in the electrolyte diffuses to the oxidized dye and regenerates it by reducing it.

The driving force for the DSC is the potential difference between the *quasi*-Fermi level, upon illumination of the working electrode, and the redox potential of the redox couple in the electrolyte. In order to be favorable for the

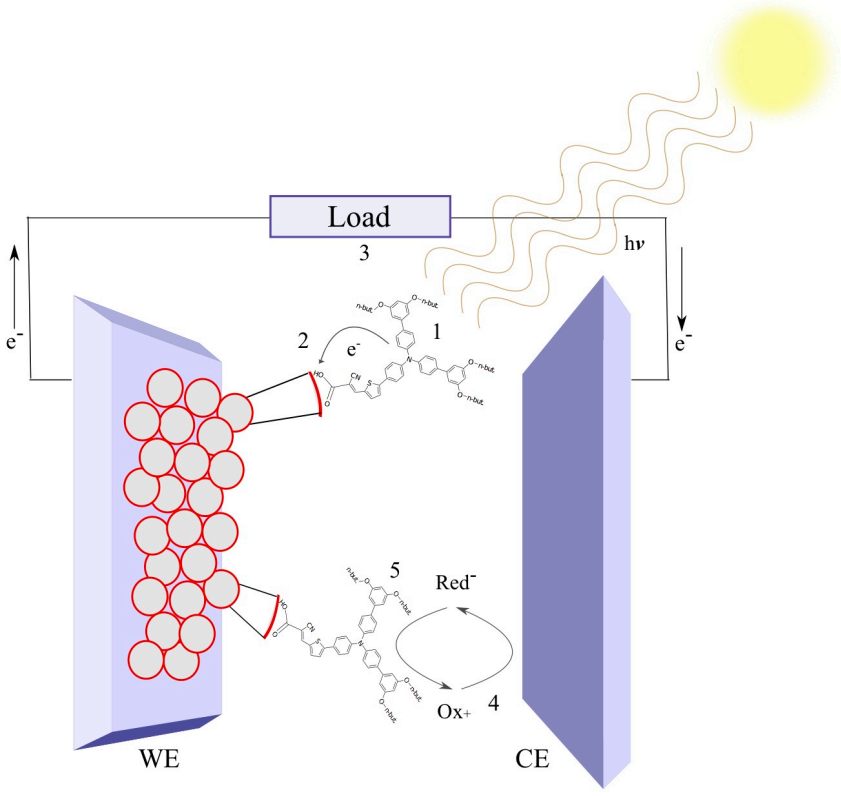

Figure 2.1. Schematic illustration of a DSC.

electrons to move into the circuit and not recombine, the forward reactions must be faster than the back-reactions. In Figure 2.2 the different time scales of the processes are put on a timeline, where it is seen that the dye regeneration is faster than the recombination of photoelectrons injected into the conduction band of TiO_2.

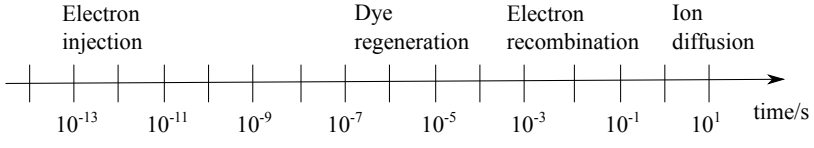

Figure 2.2. The time scale of different processes in the DSC.

In Figure 2.3 the kinetics of the DSC are illustrated. Down below follows a brief description, a review on the subject can be found elsewhere [24].

1. When the photon hits the dye, the electron is excited from the HOMO-level to the LUMO-level instantaneously.

2. One of the particular processes in the DSC is the injection of electrons into the semiconductor, which takes place within 100 fs - 100 ps. This is depending on experimental conditions and there has been discussion about the injection kinetics [24].
3. The regeneration of the oxidized dye is in the μs scale. The kinetic of the regeneration process explained by Marcus theory has been studied by Feldt and co-workers [25].
4. Process where the electron goes back to ground state, both by radiative and non-radiative processes.
5. Recombination of photo-injected electrons in the conduction band to the oxidized species in the electrolyte.
6. Recombination of photo-injected electrons in the conduction band to the oxidization level of the oxidized dye.

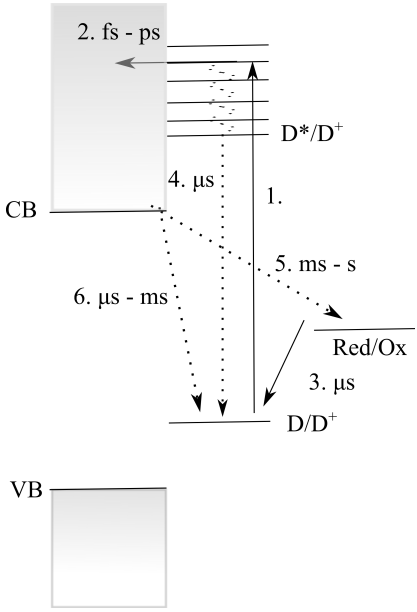

Figure 2.3. Schematic picture showing the different forward processes (solid lines) and reverse processes (dashed lines) and their time scales in the DSC.

In Figure 2.4, the different energy levels are illustrated. The DSC is a system bridging between physics and chemistry since it contains a semiconductor, TiO_2, with conduction band, normally described in relation to the vacuum level. The vacuum level refers to the energy of a free stationary electron that is outside of any material (it is in a perfect vacuum). Since the DSC also contains classical elements for electrochemistry, such as a redox couple, it is natural to relate this to the energy versus the normal hydrogen electrode (NHE). The NHE refers to a platinized high surface area electrode immersed into a solution of acid with activity of H^+ = 1 mol dm^{-3} in the presence of

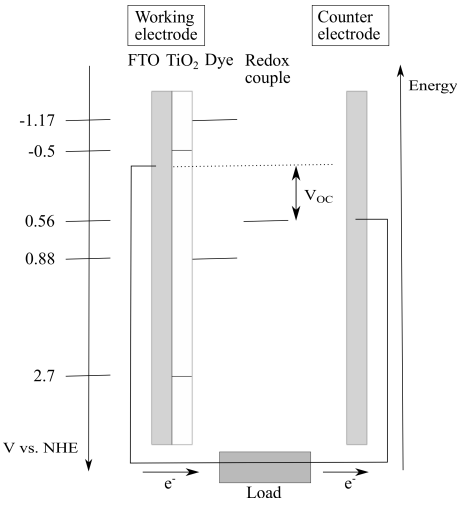

Figure 2.4. Schematic diagram of the different energy levels in the DSC. The diagram is for TiO_2, LEG4 and the redox couple $Co(bpy)_3(PF_6)_2$/$Co(bpy)_3(PF_6)_3$.

H_2 gas. Other redox potentials are related to this potential. The open circuit voltage (V_{oc} in V) of a DSC is obtained as the potential difference between the *quasi*-Fermi level in the TiO_2 (E_{F,TiO_2} in eV) and the redox potential of the redox couple ($E_{F,redox}$ in eV), see Equation 2.1, divided on the elementary charge of an electron (q in C). In dark conditions these are the same.

$$V_{oc} = \frac{E_{F,TiO_2} - E_{F,redox}}{q} \tag{2.1}$$

The redox potential, E_{redox} (in V) of the redox couple is determined by the Nernst equation:

$$E_{redox} = E^0 - \frac{RT}{nF} \times ln(\frac{a_{red}}{a_{ox}}) \tag{2.2}$$

where E^0 (in V) is the standard potential, a_{red} and a_{ox} are the activities which means the activity coefficients times the concentrations. The equilibrium Fermi level, E_f, is calculated by:

$$E_f = E_c + k_B T \times ln(\frac{n_C}{N_C}) \tag{2.3}$$

where E_c is the energy of the conduction band edge, n_C is the density of conduction band electrons and N_C is the effective density of conduction band states. The mentioned Fermi level is the level at which the concentration of the electrons is 50% of the total. In the DSC, only free electrons, i.e. the electrons that can move in the conduction band, contribute to the current in the solar cell. The injected photoelectrons in the mesoporous TiO_2 move through diffusion. The diffusion of the electrons in the TiO_2 is described by the multiple

trapping model [26]. In this model the TiO_2 is considered to contain trap levels, which are localized states below the conduction band. Electrons can only contribute to the efficiency of the solar cells if they are free and can diffuse. An illustration of this is shown in Figure 2.5.

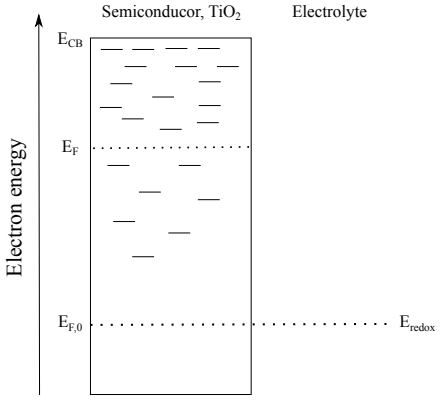

Figure 2.5. Schematic picture illustrating the semiconductor TiO_2 in contact with a redox electrolyte. E_{CB} is the conduction band of the TiO_2, E_F is the *quasi*-Fermi level upon injection of photoelectrons, in dark conditions the Fermi level, $E_{F,0}$, and the redox potential of the redox couple E_{redox} are in equilibrium.

3. Components

3.1 The working electrode

3.1.1 The nanocrystalline semiconductor electrode

In the early studies of photoelectrochemical systems a monolayer of semiconductors was used. This lead to an intrinsic limitation, as the monolayer only could absorb a limited amount of light, and only the monolayer of dye bound to the surface could inject electrons into the semiconductor. By using a mesoporous structure the surface area can be enhanced 1000-fold. A beautiful analogy is in nature, where the surface area is increased by stacking the chlorophyll containing thylakoid membranes to grana structures. In the early history of the development the DSC, many different semiconductors were used for the working electrode. In Figure 3.1 a collection of different semiconductors are illustrated.

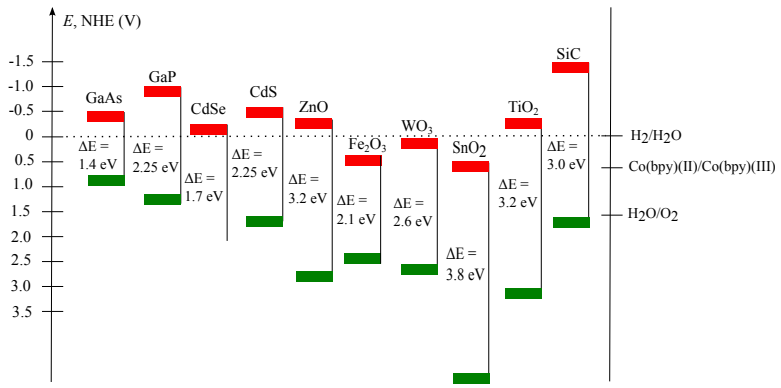

Figure 3.1. The band positions of several semiconductors in contact with aqueous electrolyte at pH 1. The conduction band edge is represented by red color and the valence band by green color. On the right side the redox potential for water oxidation, hydrogen reduction and the redox potential for the cobalt bipyridine redox couple [27].

For the porous structure to be effective the nanoparticles need to have a pathway for electrical conduction. When preparing the mesoporous TiO_2 electrodes used in this thesis, two methods have been used. A polymer solution, in which TiO_2 nanoparticles are dispersed, has been screen-printed onto the conductive glass substrate and sintered. By sintering, the organic components are burnt out, the particles "melt" together and contact is formed. On this layer

a wet chemical deposition method has been applied by immersing the samples in a $TiCl_4$ (aqueous) solution. This leads to nanocrystalline particles directly on the substrate. Further description of fabrication of the TiO_2 electrodes can be found in paper I-IV.

TiO_2 electrodes

TiO_2 is a versatile compound not only used as a semiconductor in photochemical applications. It is used in white paint, toothpaste, sunscreen and food (E171) et cetera. TiO_2 is nontoxic, stable and cheap. There is also a research field where TiO_2 is used as photocatalyst for degradation of organic pollutants in aqueous and gaseous phases, self-cleaning windows are an application of this. TiO_2 was also the semiconductor used in the famous *Electrotechnical Photolysis of Water at a Semiconductor Electrode* paper by Fujishima and Honda [28]. TiO_2 has band positions suitable for hydrogen production from water by having the valence band more positive than the redox potential for H_2O/O_2 and the conduction band more negative than the redox potential of H_2/H_2O.

TiO_2 has several crystal forms occurring naturally; rutile, anatase and brookite. Rutile is the thermodynamically most stable form but anatase is the one preferred in DSC:s. The reason is the band gap of anatase being 3.2 eV while it for rutile is 3.0 eV. The higher conduction band edge of anatase leads to higher Fermi level and higher V_{oc} in DSC application. Since no TiO_2 particles were synthesized in this thesis, description of synthesis can be found elsewhere [29]. Mesoporous TiO_2 structure composed of nanoparticles was used in the breakthrough paper by Grätzel and O'Regan [10]. Since then there has been a tremendous development of different kinds of nanostructures such as nanowires, nanorods, nanobowls, nanosheets, nanotubes and microbeats. For extensive overlook of different kinds of TiO_2 structures for DSC see reference [29].

ZnO electrodes

ZnO is very similar to anatase TiO_2 considering the valence and conduction bands, see Figure 3.1. Historically ZnO was used in the research founding the DSC field [30]. ZnO has higher electron mobility than TiO_2, which should favor electron transport. The problem with ZnO is its stability, especially in aqueous solutions. ZnO dissolves in both acidic and basic solutions and the range where it is stable is very limited. It has been noticed that dissolution of ZnO by the carboxylic acid anchoring groups take place, resulting in Zn^{2+} ions. The Zn^{2+} ions then form insoluble complexes with ruthenium dyes such as N3 and N719. These insoluble complexes precipitate in the mesoporous structure and cause charge transfer problems. Ideally for ZnO a dye without protons should bee used. It could be believed that ZnO due to the similarities in the conduction band and valence band levels with TiO_2 has been subject

for photocatalytic research, just as TiO_2. However, ZnO exhibit photo decomposition upon prolonged optical radiation. There has been extensive research nevertheless within the DSC area on ZnO, for literature see elsewhere [29].

3.1.2 Anchoring of dye to oxide surface

There are generally different kinds of adsorption modes such as covalent bonding, electrostatic interaction, hydrogen bonding, hydrophobic interaction, Van der Waal force and physical entrapment inside pores or cavities. For a DSC the linking of the dye to the semiconductor surface needs to be stable. It is therefore natural that most dyes today have an anchoring group that reacts with the semiconductor surface and creates a chemical bond, over which charge transfer takes place. Most often a carboxylic acid is used, which reacts with the hydroxyl group on the surface. There has been other anchoring groups investigated such as esters, acetic anhydride, carboxylate salts and amides [24]. The carboxylic acid anchoring group can coordinate to the oxide surface in three different ways; unidentate mode, chelating mode and bridging bidentate mode, see Figure 3.2. The mode of absorption on the oxide surface can be obtained by measuring FT-IR spectroscopy and calculating the frequency distance between the asymmetric and the symmetric stretching modes of the carboxylic acid.

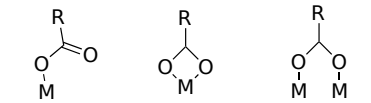

Figure 3.2. The different binding modes for the carboxylic acid anchoring group on an oxide surface.

3.2 The counter electrode

The task of the counter electrode is to reduce the oxidized species of the redox couple. This should be done with as low resistance as possible in order to attain an efficient DSC. The most common counter electrode material used for the iodide/triiodide redox system has been thermally deposited platinum nanoparticles. The thermal deposited platinum counter electrode is very efficient for the iodide/triiodide system. However, after the introduction of cobalt complexes as redox couple, it was shown that platinum was not the most efficient in the cobalt-based redox system [31]. Instead, conductive polymers such as Poly(3,4-ethylenedioxythiophene) (PEDOT) has been shown to be efficient for cobalt, as well as for sulfur-based redox couples [31, 32]. In paper

I PEDOT counter electrodes were fabricated by electropolymerization of the monomer 3,4-ethylenedioxythiophene (EDOT), and investigated in the cobalt redox couple system. There are a number of publications on different counter electrode catalysts such as carbon materials, conductive polymers, cobalt sulfide [29]. In our laboratories there has also been a thorough examination of functionalized graphene sheets[33].

3.3 The dye

The task of the dye is to absorb the photons, harvest as many as possible and inject electrons into the semiconductor. The reason why a dye-sensitized solar cell is dye-sensitized is because the band gap of the semiconductor is so wide that it only absorbs light in the UV region. In Figure 3.1 it is shown that the band gap of TiO_2 is about 3-3.2 eV. This corresponds to an absorption threshold of approximately below 400 nm. In this way a great deal of photons are lost and the efficiency will never be high. If a sensitizer is introduced, two more tunable energy level are added and higher light harvesting is achieved. There are many different kinds of sensitizers such as metal complexes, porphyrins, phtalocyanines and metal free organic dyes. For an extensive review on different kinds of sensitizers for DSC see elsewhere [29].

Most metal based dyes for DSC application are ruthenium based, they have favorable properties such as; broad absorption, suitable energy levels, relatively long lived excited state and good electrochemical stability. There are a number of articles published about ruthenium complexes [29]. Two famous ruthenium based dyes within the DSC field are; the N719 and the "Black dye". N719 was published by Grätzel and co-workers in 1997 [34] and the "Black dye" in 2001 by the same group [35]. Both N719 and the "Black dye" can be seen in Figure 3.3.

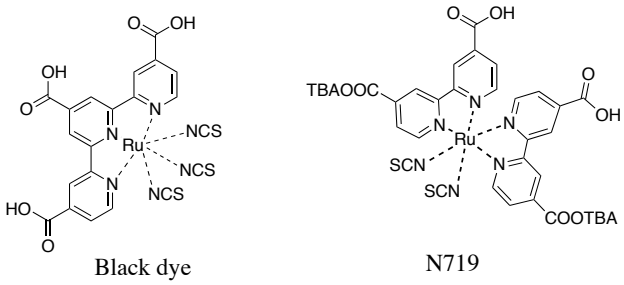

Figure 3.3. The "Black dye" and the N719 dye, both ruthenium based.

By introducing the "Black dye" Grätzel and co-workers extended the incident photon conversion efficiency (IPCE) into the IR-spectrum up to 920 nm yielding 10.4% efficiency [35]. In this thesis organic dyes were used. Organic dyes

have a number of advantages.

- They can be easy to synthesize.
- Since the metal based dyes often contain rare earth metals (Ruthenium for example) the organic ones can be cheaper and also more environmentally friendly.
- The molar extinction coefficient of organic dyes is often higher compared to metal based. This makes them suitable for solid state solar cells where the TiO_2 thickness is limited.
- With the donor-linker-acceptor concept of the organic dyes it is easy to design new dyes.

The donor-linker-acceptor dyes are, as the name suggests, molecularly designed with three different parts with distinct functions. The name donor and acceptor refers to the ability of the different parts in the molecule to donate or withdraw electron density respectively. The donor and the acceptor are linked by the π-linker. The linker influences the absorption spectrum of the dye, which is depending on the length, degree of conjugation and intrinsic electron withdrawing and donating ability of the linker. The HOMO-LUMO gap of the donor-linker-acceptor dye is largely depending on the HOMO by the donor and the LUMO on the acceptor, however this is not completely the whole truth since the linker unit inflicts on the gap between the HOMO and LUMO of the molecules as well. The acceptor is the part attaching to the semiconductor. D35 is an organic dye with donor-linker-acceptor architecture, D35 is shown in Figure 3.4. The donor unit is the triphenylamine unit, the linker is the thiophene unit and the acceptor is the cryanoacrylic acid unit.

An alternative to dye-type sensitizers are quantum dots. Quantum dots are interesting due to their intrinsic properties. The band gap vary with size, therefore absorption and redox properties can be tuned by the synthesis of the quantum dots [12, 13].

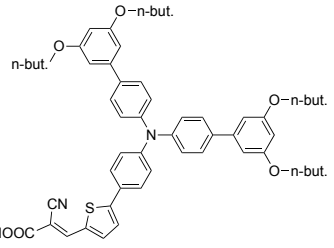

Figure 3.4. The organic donor-linker-acceptor dye D35.

3.4 The redox couple

Iodide/triiodide was the redox couple used in the breakthrough article of 1991 [10]. However, iodide/triiodide as a redox couple has some disadvantages, one of them being a lower redox potential ($\sim$ 0.35 V versus NHE) than necessary for dye regeneration limiting the V_{oc} and hence also the η [36]. Normally the dyes have HOMO levels of about 1 V versus NHE leaving a potential difference of about 0.75 eV. Another disadvantage is the high molar extinction coefficient, thereby limiting the light harvesting efficiency of the system. Today the world record efficiency of 13% for DSC:s is obtained with a cobalt complex [37]. Cobalt as a redox mediator had a breakthrough in 2010 when Feldt and co-workers introduced a combination of dye and redox couple that decreased the recombination [38]. Since the paper by Feldt and co-workers there has been a number of different cobalt complexes studied [25, 31]. Cobalt complexes open up the possibility to tune the redox potential and thereby optimize the kinetics of the regeneration. The driving force necessary for regenerating of the dye has been studied [25], for most cobalt complexes studied it was concluded that the regeneration efficiency decreased when the driving force decreased below 0.4 eV. The iodide and cobalt complex redox mediator systems differ in the cobalt being a one electron process while the iodide has a many step process. It has been presented that the iodide/triiodide couple regenerates the dye, D, most likely in a sequence of reaction steps [29, 39]. See the following mechanism.

$$(D^{+} + I^{-}) \rightarrow (D \cdots I) \tag{3.1}$$

$$(D \cdots I) + I^{-} \rightarrow (D \cdots I_2^{-\bullet}) \tag{3.2}$$

$$(D \cdots I_2^{-\bullet}) \rightarrow D + I_2^{-\bullet} \tag{3.3}$$

$$2I_2^{-\bullet} \rightarrow I_3^{-} + I^{-} \tag{3.4}$$

3.5 Electrolyte solvent

In the beginning of the DSC history water was used as electrolyte solvent. These systems achieved however modest efficiencies of 1-2% with illumination of less than 1 sun [40, 41]. Water has many advantages as solvent, one of them being that the conduction band in colloidal TiO_2 anatase particles can be controlled. It has been shown that the conduction band depends on pH by [42]:

$$E_{CB} = 0.1 + 0.059 \times pH(eV, NHE) \tag{3.5}$$

Table 3.1. *Physical properties of solvents used for electrolytes in DSC.*

Solvent	mp/bp (°C)[b]	ε_r^c	viscosity (mPa s)[d]	$D^e_{I_3^-}$ ($cm^2\ s^{-1}$)
water	0/100	80	0.89	1.1×10^{-5}
ethanol	-114/78	24	1.07	-
acetonitrile	-44/82	36.6	0.34	1.5×10^{-5}
propionitrile	-92/97	28	0.41	-
valeronitrile	-96/140	20	0.71	-
glutaronitrile	-29/286	37	5.3	-
methoxyacetonitrile	/119	-	-	7.6×10^{-6}
3-methoxypropionitrile	-57/165	36	1.1	$4\text{-}5 \times 10^{-6}$
γ-butyrolactone	-44/204	42	1.7	3.9×10^{-6}
propylene carbonate	-49/242	65	2.5	$2\text{-}3 \times 10^{-6}$
PMImI[f]	-55/	-	880[f]	1.9×10^{-7}

[a] melting/boiling point at 1 atm. [b] Relative dielectric constant.
[c] Viscosity at 25 °C of the pure solvent (mPa s = cP). [d] Apparent diffusion coefficient for triiodide in a DSC electrolyte. $D_{I_3^-}$ will depend on electrolyte composition. [e] 1-Methyl-3-propylimidazolium iodide (ionic liquid).
[f] with 0,05 M I_2 added.

as the pH increase the conduction band will move towards more positive values. This affects the kinetics of the DSC. As time moved into the 1990:s water was replaced by organic solvents. In Table 3.1 solvents used for DSC are listed. The table is adopted from the review by Hagfeldt and co-workers [29], in the same review different solvents for DSC:s are discussed more comprehensively.

The demands on the solvent for the electrolyte in the DSC is that it should be chemically stable, have a low viscosity and provide good solubility for the redox mediator and other additives in the electrolyte. It is also important that the solvent does not cause desorption of the dye, semiconductor or dissolve the sealing material. The solvents most frequently used today are relatively polar organic solvents, for example acetonitrile. In the 1991 Nature article by Grätzel and O'Regan a mixture of ethylene carbonate and acetonitrile was used. 3-methoxypropionitrile (MPN) is good for stability studies due to its low vapor pressure. Acetonitrile is a commonly used solvent today, the world record is performed with this solvent [37]. The problem with acetonitrile is however the vapor pressure which could cause long term stability problems for modules. Extensive research for finding less volatile solvents has been performed. Ionic liquids possess low vapor pressures and have shown giving stable systems [21, 29]. Electrolytes can also be based on both organic solvents and ionic liquids, these electrolyte mixtures can be gelated, polymer-

ized, or dispersed with polymeric materials. This gives something called a *quasi*-solid electrolyte. The advantage of the ionic liquid and the *quasi*-solid based electrolytes is the lower vapor pressure and thereby the stability. The disadvantage is the mass transport limitations.

As already mentioned water was used as solvent in the beginning of the DSC history. After the introduction of organic solvents water started to be considered a problem in DSC:s. The presence of water in the DSC has been reported to degrade organic solvent-based electrolytes due to the formation of iodate [43], detachment of dye [44, 45] and reducing the electron lifetime [46]. Water should however be an excellent solvent for electrolytes in DSC as it is non-toxic, non-flammable and compared to the most used solvent today, acetonitrile, it possess lower vapor pressure. Another consideration is the stability. Water will most probably permeate into the solar cell modules with time, if not extensive permeation barriers are added to the design. With water as electrolyte solvent permeation of water would not be a problem. Another advantage of water would be the cost, as water is cheaper than organic solvents. After the breakthrough with organic solvents, water was put aside as solvent. Until 2010 there were few articles examining water as electrolyte solvent for the DSC. After 2010 there has been some articles published with water-based DSC:s [47, 48, 32, 49, 50]. These papers gave inspiration for the study in paper III of this thesis.

The intrinsic problem of using water as electrolyte solvent for the iodide/triiodide redox mediator system could be due to how water as solvent affects the mechanism seen by Equation 3.1, Equation 3.2, Equation 3.3 and Equation 3.4. Hagfeldt and co-workers argue that the difference between the formal reduction potential of $I_2^{-\bullet}/I^-$ and D^+/D determines the driving force for regeneration of the dye [39]. Hagfeldt and co-workers determined the value of $E^{0'}$ ($I_2^{-\bullet}/I^-$) in water to +1.04 V versus NHE, comparable to the value in acetonitrile +0.79 V. Water as solvent shift the redox potential to a more positive value, lowering the driving force for regeneration of the dye in water. Another disadvantage of using water as electrolyte solvent for the iodide/triiodide redox mediator system could be the binding coefficient of I^- and I_2 to form I_3^- (Equation 3.6). In water $K_M = \sim 1000$ compared to $K_M = \sim 4 \times 10^6$ in acetonitrile. The concentration of I_2 thus being unavoidably higher in water-based iodide/triiodide electrolytes, compared to equivalent acetonitrile electrolytes. The main pathway for recombination in cells with iodide/triiodide electrolytes in MPN and propylene carbonate has been shown to be the reduction of I_2 [51]. This presents another intrinsic limitation of low V_{oc} in water-based iodide/triiodide redox mediator DSC.

$$I^- + I_2 \rightarrow I_3^- \tag{3.6}$$

4. Characterization techniques

4.1 Characterization of complete device

4.1.1 Current-voltage characteristics

One of the most essential measurements of a solar cell is the current-voltage (I-V) measurement. In order to be able to compare performances of solar cells the IV curve is measured under illumination of a lamp with a spectrum similar to the AM1.5G illumination. The AM1.5G spectrum is the spectrum of sunlight that has traveled 1.5 times the thickness of the atmosphere. The intensity of the illumination is calibrated to 1000 W/m^2, equal to 1 sun. The IV characteristics are monitored under illumination by applying an external potential between the working and counter electrode. The external potential is altered from J_{sc} to V_{oc} or opposite depending on scanning direction. The IV curve can also be measured under dark conditions. This will give information about recombination to the oxidized redox species. Since no oxidized dye is present in dark, the dark current is a measure of electrons going in the reverse way, from the TiO_2 to the oxidized species of the redox couple. An example of IV curves performed under 1 sun and in dark is shown in Figure 4.1.

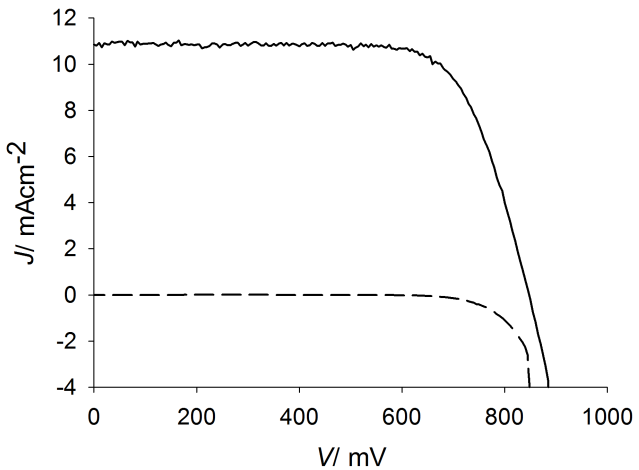

Figure 4.1. IV curve of the LEG4 dye under 1 sun illumination (solid) and in dark (dashed).

The IV measurements should be carried out with enough slow scan rate so the solar cell has time to adjust and no hysteresis effects appear. The maximum power point is given by the P_{max} values. By this the fill factor (FF) is

introduced, the FF is a measure of the ratio of the P_{max} and J_{sc} and V_{oc} see Figure 4.2.

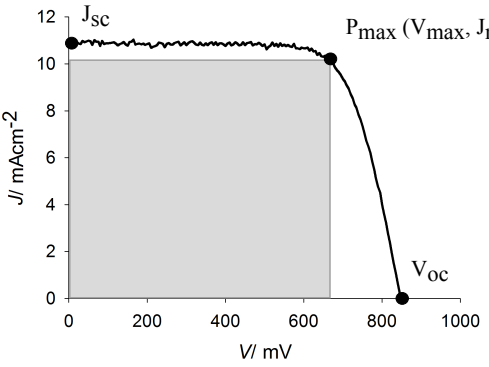

Figure 4.2. IV curve of the LEG4 dye under 1 sun illumination. By taking the area of the shaded square and dividing it by the area of the one covered by the V_{oc} and the J_{sc} the FF is obtained.

The efficiency of a solar cell is calculated as the ratio between the output power and the input energy:

$$\eta = \frac{P_{max}}{P_{in}} = \frac{J_{sc} \times V_{oc} \times FF}{P_{in}} \tag{4.1}$$

where FF is relating the P_{max}, J_{sc} and V_{oc} according to the following equation.

$$FF = \frac{J_{max} \times V_{max}}{J_{sc} \times V_{oc}} \tag{4.2}$$

The inclination of the IV curve is related to the resistances in the solar cell. In paper I the FF was used as a measure of how the different kinds of counter electrodes affected the resistance of the solar cells.

By measuring the IV curve with electrolyte sandwiched between two conductive electrodes, the diffusion coefficient of the oxidized species of the redox couple can be determined. This was utilized in paper I (see chapter 5) to determine the diffusion coefficient of the oxidized species in the cobalt electrolyte.

4.1.2 Incident photon to current conversion efficiency

The incident photon to current conversion efficiency (IPCE) is a measure of the efficiency of the solar cell to convert the incoming photons to photocurrent at different wavelengths. This is done by measuring the resulting photocurrent of the solar cell when illuminated by monochromatic light. The IPCE is a measure of the product of different efficiencies such as Light Harvesting Efficiency (LHE), the quantum yield of electron injection from the excited dye

into the TiO_2 conduction band ϕ_{inj}, the efficiency of regeneration η_{reg}, and the collection efficiency of the photo-generated charge carriers η_{coll}.

$$IPCE = LHE \times \phi_{inj} \times \eta_{reg} \times \eta_{coll} \tag{4.3}$$

For calculating the IPCE experimentally one use the following equation:

$$IPCE = \frac{1240 \times J_{sc}(mAcm^{-2})}{\lambda(nm) \times P_{in}(mWcm^{-2})} \tag{4.4}$$

In Figure 4.3 the IPCE spectra of two organic dyes, D35 and LEG4, in cobalt redox mediator based DSC:s are shown.

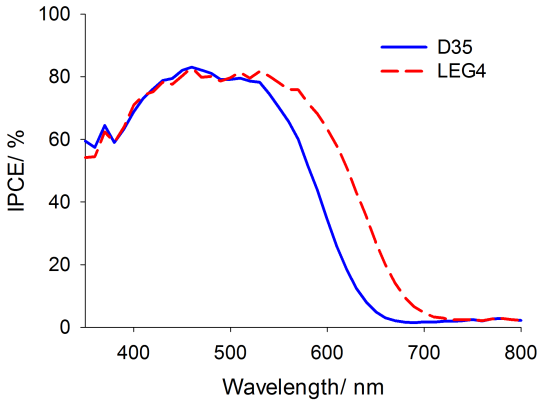

Figure 4.3. IPCE spectra of the two organic dyes, D35 and LEG4, in cobalt redox mediator based DSC:s.

4.1.3 Toolbox techniques

Toolbox techniques is a generic way of addressing measuring techniques that measure; electron lifetime, transport time and extracted charge. All toolbox measurements in this thesis were measured with a system described by Boschloo and co-workers [52]. In short the measurements were performed using a white LED as light source. Voltage and current traces were recorded with a 16-bit resolution digital acquisition board in combination with a current amplifier and a custom made system using electromagnetic switches. It should be pointed out that by using the toolbox techniques for measuring the electron lifetime and the transport time different conditions are applied. Electron lifetime is measured under open circuit conditions while the transport time is measured under short circuit conditions. The parameters are therefore not measured under working conditions.

Electron lifetime measurements
In the electron lifetime measurement the lifetime of the electrons in the TiO_2, before recombining to the oxidized species in the electrolyte, or to the oxidized dye, is measured. The experiment is carried out by applying a small modulation with a certain frequency to the bias voltage applied to the light source. The resulting rise and fall to a new open circuit voltage of the solar cell as a response to the modulation of the bias voltage of the light source is measured. The corresponding rise and fall times are calculated with aid of fitting. The electron lifetime is obtained by averaging the rise and fall times. The electron lifetime is an important parameter to measure when evaluating different redox couples. Before Feldt and co-workers published their study of cobalt polypyridine redox mediators in 2010 [38] the problem of alternative redox couples to iodide/triiodide had been the short electron lifetimes and fast recombinations to one electron redox mediator. In the study by Feldt and coworkers it is shown how the dye design can be used to decrease recombination and increase electron lifetime.

Electron transport measurements
In the transport time measurement the time it takes for the electrons to travel to the back-contact of the working electrode is measured. The experiment is carried out by applying a small modulation with a certain frequency, to the bias voltage applied to the light source. The solar cell is kept at short circuit conditions. The resulting rise and fall to a new short circuit current as a response to the modulation of the bias voltage of the light source is measured. The corresponding rise and fall times are calculated with aid of fitting. The transport time is obtained by averaging the rise and fall times. Transport time measurements can be used to evaluate the conduction of electrons in the semiconductor.

Extracted charge measurements
Extracted charge measurements can be carried out both at open circuit and at short circuit conditions. At open circuit conditions the solar cell is illuminated at open circuit conditions, after a certain time the light is turned off and simultaneously the solar cell is switched to short circuit conditions while the current is monitored. The extracted charge during the short circuit conditions is obtained by integrating the current with time. At short circuit conditions the solar cell is illuminated under short circuit conditions. The current is monitored though a current amplifier. After a certain time the illumination is turned off and the software integrate the current with time. Extracted charge measurements can be used to see if the conduction band is shifted. This was done in paper II. In Figure 4.4c the extracted charge as a function of V_{oc} is shown. The measurement shows that the different dyes anchored on the surface do not shift the conduction band of the TiO_2. In Figure 4.4d the extracted charge for the LEG-series of dyes is illustrated but at short circuit conditions.

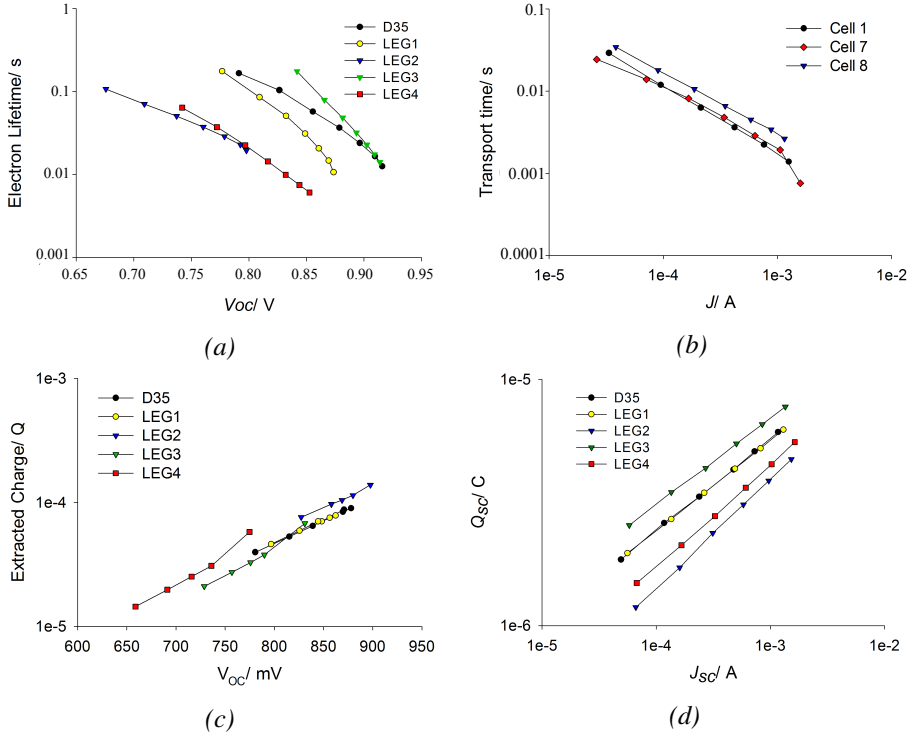

Figure 4.4. Toolbox measurements. Figure (a) shows lifetimes of the LEG-series of dyes. Figure (b) shows transport times of ZnO working electrodes covered with different layers of MgO sensitized with D35 and cobalt electrolyte. Figure (c) shows extracted charge of the LEG-series of dyes at open circuit conditions. Figure (d) shows the extracted charge of the LEG-series of dyes at short circuit conditions.

4.1.4 Impedance spectroscopy

The purpose of a solar cell is to generate electrons, current and voltage. For this to be as efficient as possible there should be as few losses and as little resistance for the charge transfer processes in the solar cell, as possible. Lower resistance within the cell will also minimize voltage drops. The IV curve gives by the inclination to the V_{oc} the total resistance in the solar cell.

$$\frac{dI(V)}{dV} = \frac{1}{R_{tot}} \tag{4.5}$$

However, this is the total resistance in the solar cell and does not give any information about the resistances in the different components such as charge transfer at the counter electrode, resistance of electron transport in the TiO_2, recombination resistance or diffusion resistance in the electrolyte. By measuring electrochemical impedance spectroscopy (EIS) one can obtain information about different components' resistance and capacitance. In the DSC there are

resistances for the charge transfer processes at the FTO glass, giving rise to the series resistance R_s, at the TiO_2/dye surface - electrolyte giving the recombination resistance, R_{rec}. A high R_{rec} is good since this implies that the resistance for recombination of injected electrons in the conduction band of the TiO_2 with the oxidized species of the redox couple is high. There is also resistance in the electrolyte due to diffusion of the redox couple. This is given by the Warburg element. At the counter electrode there is the resistance for the charge transfer process of the reduction of the oxidized species in the electrolyte. In the DSC there is double layer capacitance, this occur due to the charged surfaces at the working and counter electrode. At the working electrode the injected electrons charge the surface negatively, positively charged cations in the electrolyte are attracted and a Helmholtz layer is created generating double layer capacitance. The counter electrode experience the same phenomena and also here a double layer capacitance is built up. Resistance is the ability of an electric circuit to resist the flow of electrical current, electrons. Ohm's law gives the relationship between current, voltage and resistance.

$$V = I \times R \tag{4.6}$$

Impedance is introduced when working with AC signals. Under such conditions, current can flow through a capacitor, which is depending on the AC frequency. By applying a sinusoidal alternating potential to the electrochemical system and measuring the output, a sinusoidal current, one obtains the impedance. Since the input, the voltage, and the output, the current will be phase shifted it is convenient to describe impedance by complex numbers.

$$z = x + jy \tag{4.7}$$

where

$$j = \sqrt{-1} \tag{4.8}$$

Impedance is represented by a real and an imaginary part. One often describe the real part as the magnitude |Z| and the imaginary part as the phase θ.

$$Z = |Z| \times e^{j\theta} \tag{4.9}$$

$$Z = |Z|cos(x) + |Z|jsin(x) \tag{4.10}$$

$$Z = Real(Z) + Imaginary(Z) \tag{4.11}$$

When measuring impedance of a DSC and plotting the imaginary part (capacitance) on the y-axis and the real part (resistance) on the x-axis, this is called a

Nyquist plot. When measuring a standard DSC half circles will appear in the spectrum. A standard Nyquist plot of a DSC is shown in Figure 4.5.

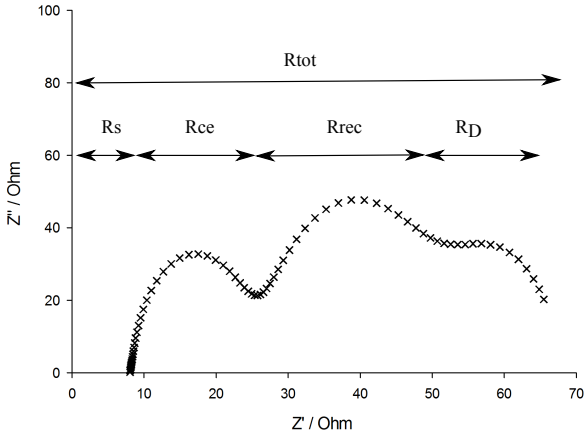

Figure 4.5. Resistances in a DSC. The total resistance, R_{tot}, is depending on the series resistance R_s, the charge transfer resistance at the counter electrode R_{ce}, the recombination resistance of electrons in the TiO_2 conduction band to the redox couple in the electrolyte R_{rec} and the diffusion resistance for the redox couple in the electrolyte, R_D.

In the Nyquist plot the x-axis gives the real part of the impedance the |Z|-value and the y-axis the imaginary part, the phase θ. One normally scans from low frequencies to high frequencies. For a DSC the first resistance that the will appear is the R_s, the resistance between the FTO-glass and the TiO_2. This is real and is where the measurement points start in the spectrum. After this a first semicircle appear. This illustrates R_{ce}. The impedance contains both the double layer capacitance of the counter electrode and the resistance for the electron transfer. This gives both an imaginary and a real part. As starting at low frequencies the capacitance will be 0 and working as a resistor. As the frequency increase the capacitor starts to behave as a capacitor, loading and de-loading. This gives the phase angle θ, the imaginary part. At a certain frequency the maximum θ is reached and the angle decrease again. The second semicircle appearing is the TiO_2/dye surface - electrolyte interface, the R_{rec}. Here the real part gives the recombination resistance and at maximum θ the electron lifetime in the TiO_2 conduction band can be calculated. The third semicircle gives the R_D of the redox couple in the electrolyte. If a porous counter electrode is used a last semicircle can appear giving the diffusion resistance in the counter electrode of the redox couple.

Analysis of EIS for DSC

It is important to do correct measurements but also to do correct interpretation of data. For interpretation of impedance measurements a fit of the data by an

electric circuit, the equivalent circuit is done. For DSC:s a commonly used equivalent circuit is shown in Figure 4.6.

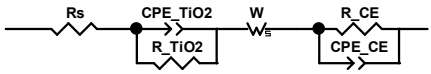

Figure 4.6. Equivalent circuit used for DSC.

As already described there is a resistor for the series resistance, for the interface TiO_2/dye surface - electrolyte there is a constant phase element and a resistor in parallel. There is a Warburg element for describing the diffusion resistance. For the interface counter electrode - electrolyte there is once more a constant phase element and a resistor in parallel. By using this model values of the different elements can be obtained. In paper I impedance was utilized to analyze the difference in charge transfer resistance at platinized counter electrodes and electropolymerized PEDOT counter electrodes. In Figure 4.7a and Figure 4.7b impedance measurements with fits by using the equivalent circuit in Figure 4.6 are illustrated. The fits show good agreement with the measured values.

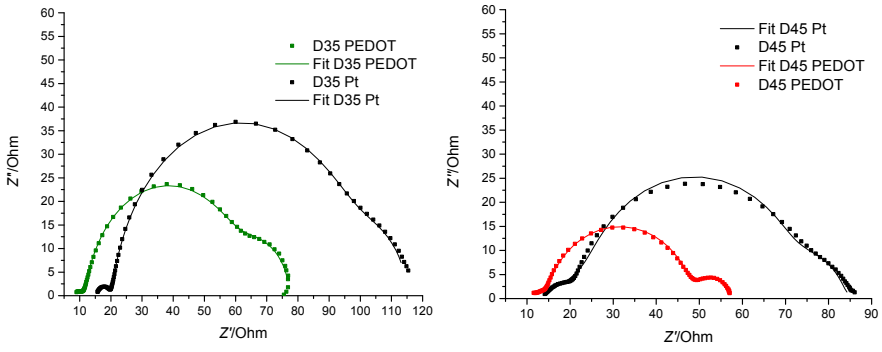

(a) *(b)*

Figure 4.7. Figure (a) shows impedance measurements with the fits for platinized and PEDOT counter electrodes used in a D35 dye DSC system. Figure (b) shows the impedance measurements with the fits for platinized and PEDOT counter electrodes used in a D45 dye DSC system. In both systems is it possible to see the difference in charge transfer resistance at the counter electrode for the platinized and PEDOT electrodes. The platinized electrodes give higher charge transfer resistance.

By measuring impedance it is also possible to obtain information about electron lifetimes in the TiO_2 conduction band. By taking the maximum angular frequency value from the second semicircle and inverting the value the electron lifetime is calculated. An example of this is illustrated in Figure 4.8.

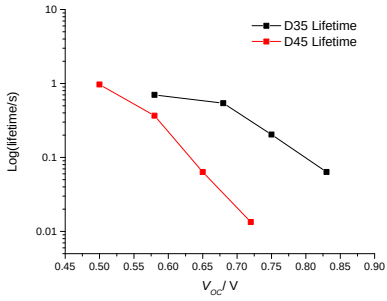

Figure 4.8. Electron lifetimes in solar cells assembled with the organic dyes D35 or D45 determined by impedance spectroscopy.

The diffusion coefficient for the redox couple can be calculated by:

$$\omega_d = \frac{D}{L^2} \tag{4.12}$$

where L is the diffusion length, D the diffusion coefficient. ω_d is the maximum angular frequency value of the third semicircle [53]. There is additionally a way of obtaining the diffusion coefficient from EIS measurements:

$$R_D = \frac{RTL}{z^2F^2aCD} \tag{4.13}$$

where R_D is the diffusion resistance, R is the gas constant, T is the temperature, L is the diffusion length, z is the number of charges transfered by the diffusing species, F is the Faraday constant, a is the electrode area, C is the concentration of the diffusing species and D is the effective diffusion coefficient of the diffusing species. This equation is though only valid for ideal solutions [54].

In this thesis impedance measurements were performed and merely the R_{ce} and capacitance at the counter electrode were derived. This was performed with symmetric cells in order to simplify the analysis and minimize the error. For fundamental description and profound work of EIS with DSC systems see elsewhere [55, 56].

4.2 Characterization of components

4.2.1 UV-visible spectroscopy

UV-vis spectroscopy is a technique for measuring absorbance as a function of wavelength. A sample is irradiated with an intensity of UV-vis light and the intensity after the sample is measured. Absorbance is defined as:

$$A = log_{10}(\frac{I_0}{I}) \tag{4.14}$$

where I_0 is the intensity of light before the sample and I is the intensity to the detector after the sample. It is evident that the greater the absorbance, the less is transmitted to the detector. The less photons that are transmitted to the detector the greater the insecurity of the measurements gets and it is recommended that an absorbance of less than 1 is used. Transmission reflects how much is transmitted by the sample instead for absorbed. Transmission, T is defined as following.

$$T = \frac{I}{I_0} \tag{4.15}$$

Absorbance A, is connected to the concentration C, of the sample, the molar extinction coefficient, ε and the length for the light to travel, L by Lambert Beers law.

$$A = C \times \varepsilon \times L \tag{4.16}$$

In a solar cell photons are converted to electrons. It is therefore desired that as many photons as possible are absorbed. UV-vis spectroscopy is therefore a commonly used technique to evaluate dyes and their possibility to absorb photons at different wavelengths. By measuring the absorbance of sensitized TiO_2 films, it is possible to determine the light harvest efficiency (LHE), see Equation 4.17.

$$LHE(\lambda) = 1 - 10^{-A(\lambda)} \tag{4.17}$$

In Figure 4.9 the LHE for the LEG-series of dyes is plotted. The full formula of the LHE is:

$$LHE(\lambda) = 1 - T - R \tag{4.18}$$

where T is the transmitted light and R is the reflectance. In Equation 4.17 R is assumed to be 0.

UV-vis spectroscopy and Lambert Beers law can be used to calculate dye coverage on the TiO_2 films. By absorbing the dye on the TiO_2 films, desorb the dye in base solution (tert-butylamonium hydroxide (TBAOH) for example) and measure absorbance of the solution, the concentration can be attained by

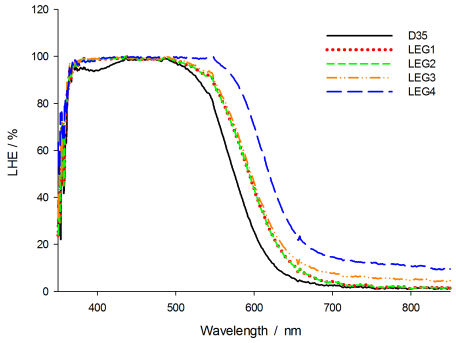

Figure 4.9. Light harvesting efficiency of the LEG-series of dyes.

Lambert Beers law. If the molar extinction coefficient, ε, of the dye in the base is known, the concentration can can be calculated according to Equation 4.16. The surface coverage on the TiO_2 is given in mol cm^{-2}. By taking the concentration obtained, and multiplying by the volume of the TiO_2, dividing this by the surface area of the TiO_2, the surface coverage is calculated.

4.2.2 Fluorescence spectroscopy

Fluorescence spectroscopy measures the emitted photons upon illumination as a function of wavelength. By illuminating molecules, photons are absorbed and electrons excited to higher energy levels. When relaxing down to the ground state, molecules emit photons of lower energy than the first absorbed energy. In DSC it is often of interested to know the gap between the ground state level and the first excited level of a dye, the E_{0-0} value. The value of this gap is essential for the absorbance of the solar cell. The gap is estimated by the intercept of the absorbance and the fluorescence spectra of the dye. Example of fluorescence spectra is illustrated in Figure 4.10. By taking the intercept of the fluorescence spectrum and the aborbance spectrum, plotted in the same graph, the gap between the LUMO and the HOMO of the dye can be estimated, see Figure 4.10.

When measuring fluorescence it is important to use low concentrations so that energy transfer is avoided. If highly concentrated samples or turbid samples are used, inner filter effects affecting the fluorescence spectrum can occur. It is necessary to pay attention to the choice of solvent so that solvent effects are considered. Since an excited molecule almost always has a higher dipole moment compared to non-excited, the excited state will be stabilized the more polar the solvent is. The more stabilized the excited state gets due to the solvent, the more red shifted the fluorescence spectrum gets. One should thereby always try to measure the absorption, fluorescence and cyclic voltammetry in

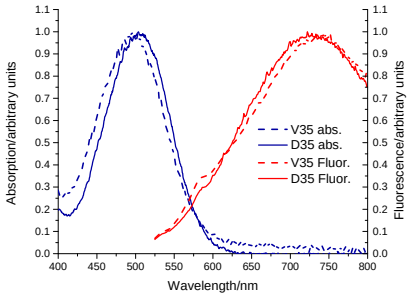

Figure 4.10. Absorbance and fluorescence of the D35 dye and the V35 dye.

the same solvent, in order to accurately determine the oxidation potential, first excited state level and the gap between them.

4.2.3 Electrochemistry

In this thesis the electrochemical measurements performed were: cyclic voltammetry for measuring the redox potential of the dyes and redox couples, limiting current measurements with microelectrodes for determining diffusion coefficient and galvanostatic measurements for electropolymerization of EDOT.

Determining the redox potential

For a DSC to be as efficient as possible, attention should be drawn to the energy levels in the system. The oxidation potential of the dye and the redox potential of the redox couple determine the driving force for regeneration of the oxidized dye. There is a trade off between efficient regeneration and loss in V_{oc}. For a dye, the oxidation potential can be determined by measuring the cyclic voltammetry of the dye in solution or attached to TiO_2. When measuring cyclic voltammetry, the potential is scanned and the resulting current from the electrochemical system is measured. The scan is sweeped, if the system is reversible an oxidation peak and an reduction peak appear. The separation between the oxidation and reduction peak for a reversible one-electron system at 298 K should be 59 mV [57] according to Equation 2.2. The cyclic voltammetry measurements performed in this thesis were performed with a three-electrode setup. Different types of electrodes were used, for example glassy carbon as working electrode, carbon as counter electrode and a reference of $Ag/AgNO_3$ (10 mM $AgNO_3$, 0.1 M $LiClO_4$). For convenience, the potentials are reported versus a reference, such as the normal hydrogen electrode (NHE). For as accurate measurements as possible, the measurements should be carried out at conditions as similar to in the DSC as possible. It is convenient to use the same additive, $LiClO_4$, often used in the solar cell electrolyte, in the cyclic voltammetry measurement.

$E^{0'}$, the formal potential is calculated by taking the average of the oxidation peak potential E_{ox} and the reduction peak potential E_{red} as seen in Equation 4.19.

$$E^{0'} = \frac{E_{ox} + E_{red}}{2} \tag{4.19}$$

This is for a reversible system meaning that both oxidation and reduction occur. In Figure 4.11 cyclic voltammetry of the calibration compound ferrocene and the dye V35 are shown. Since both systems are reversible, the redox potential can be calculated according to Equation 4.19.

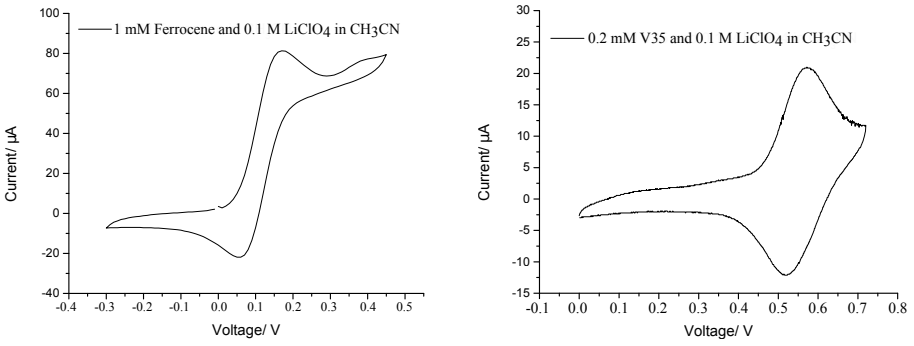

(a) *(b)*

Figure 4.11. Figure (a) cyclic voltammetry of 1 mM Ferrocene and 0.1 M $LiClO_4$ in CH_3CN, this is normally used as a reference for calibration. Figure (b) cyclic voltammetry of 0.2 mM V35 and 0.1 M $LiClO_4$ in CH_3CN.

An illustration of how to calculate the redox potential of the dye versus NHE is visualized in Figure 4.12. The difference between the reference electrode (Ag/Ag^+) and the ferrocence is taken from Figure 4.11a and the difference between the reference and the dye is taken from Figure 4.11b. There are other techniques which gives better resolution of the oxidation peak such as differential pulse voltammetry and quare wave voltammetry, the problem is that these techniques do not give information about the reversibility [29].

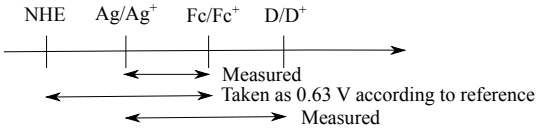

Figure 4.12. Calculating the measured redox potential versus the reference electrode versus the NHE. Ferrocene versus NHE was taken as 0.63 Volt[58].

Determining the diffusion coefficient

The diffusion coefficients of redox components in a DSC system can be determined by measuring limiting currents with microelectrodes. A compound with known diffusion coefficient is first used to measure limiting current and determining the radius of the microelectrode, a compound often used is K_3FeCN_6. With this known, the limiting current measurement are repeated with the redox components. The equation used for determining the radius of the microelectrode and the diffusion coefficients is:

$$i_{lim} = 4nFDCr \tag{4.20}$$

where n is the number of electrons in the redox reaction, F the Faraday constant, D the diffusion coefficient, C the concentration of the reacting species, r the radius of the microelectrode. In Figure 4.13a the limiting current measurement of K_3FeCN_6 is plotted and in Figure 4.13b the limiting current measurement of $Co(bpy)_3(PF_6)_2$ and $Co(bpy)_3(PF_6)_3$ is plotted.

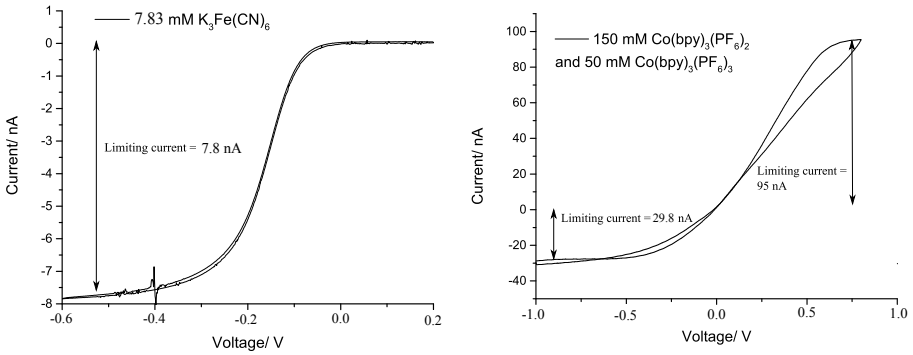

(a) *(b)*

Figure 4.13. Figure (a) measuring the limiting current of 7.8 mM K_3FeCN_6 in 0.5 M KCl, 1 mM HCl in CH_3CN. Limiting current measurement for calibration of diameter of the micro-disk. Figure (b) measuring the limiting current of 150 mM $Co(bpy)_3(PF_6)_2$ and 50 mM $Co(bpy)_3(PF_6)_3$ in CH_3CN. Measurement for determining the diffusion coefficient of $Co(bpy)_3(PF_6)_2$ and $Co(bpy)_3(PF_6)_3$.

4.2.4 Photo-induced absorption spectroscopy

Photo-induced absorption spectroscopy (PIA) is a pump probe techniques where a laser diode (green 530 nm or blue 460 nm in this thesis) is square-modulated for pumping the dye to excitation. A probe light is superimposed. When excitation takes place, the injection of electrons into the TiO_2 conduction band occurs within femtoseconds. The oxidized dye is quickly regenerated, if a redox couple is present. If no redox couple is present or the redox couple is

unable to regenerate the dye, the probe will probe the oxidized dye. The transmitted signal from the sample is focused onto a monochromator and detected using a UV-enhanced silicon photo-diode, connected to a lock-in amplifier, via a current amplifier. A more comprehensive description of the PIA setup and theory can be found elsewhere [59, 60]. A general illustration of the PIA setup is shown in Figure 4.14.

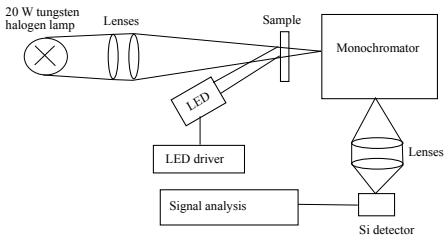

Figure 4.14. Schematic drawing of the PIA setup used for measurements in this thesis.

In Figure 4.15 a PIA spectrum of the organic dye D35 is shown. No redox couple is added and the spectrum is therefore of the oxidized dye. There is a negative absorption peak at about 550 nm, this correspond to the ground state bleach and occur due to all dye molecules not being pumped to excited state. Some dye molecules remain in the ground state and absorb when the probe illuminates the sample. The ground state bleach is an inverse absorption peak. In this region of the ground state bleach also the Stark effect can be observed. The Start effect is due to the oxidized dye molecules on the TiO_2 impose a change in the local electric field. The Stark effect is described in detail elsewhere [60]. In short the absorption spectrum of the dye molecules shift due to the local electric field caused by the oxidized molecules. The positive signals, as moving towards longer wavelengths, are of the absorption of the oxidized dye molecules.

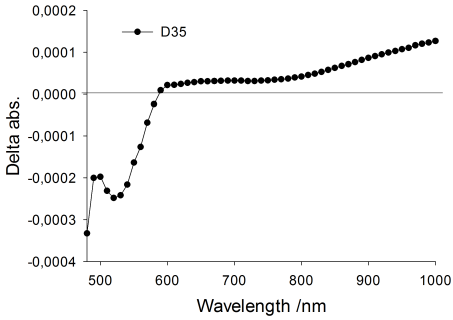

Figure 4.15. PIA spectrum of the organic dye D35 without redox couple present.

PIA was in this thesis used to study regeneration of the oxidized dye and to find the wavelength where the oxidized dye absorb.

4.2.5 Transient absorption spectroscopy

Transient absorption spectroscopy (TAS) is a pump probe technique, just as PIA previously described. The difference between the transient nanosecond laser measurements and the photo-induced absorption measurements is the time scale. In the transient nanosecond laser measurements the resolution in time is better, regeneration can be studied and the time constants for the regeneration can be derived. With photo-induced absorption measurements only information whether regeneration takes place or not can be attained, not at what time scale the regeneration takes place (not with the standard apparatus used in this thesis). A schematic drawing of a nanosecond transient absorption apparatus used in this thesis is illustrated in Figure 4.16. Transient nanosecond laser measurements are often used in investigations of kinetics of DSC:s.

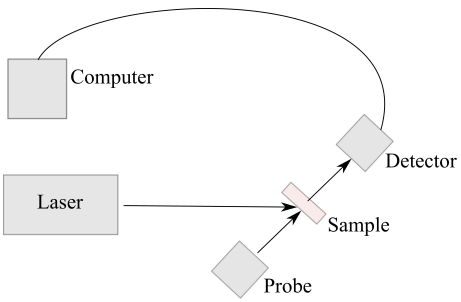

Figure 4.16. Apparatus for transient absorption measurements. The laser used in the measurements for this thesis was a Nd:YAG with a 10 ns pulse width.

In paper II TAS measurements were carried out in order to measure the difference in regeneration and recombination of the LEG-series of dyes. In Figure 4.17 the decay of the absorption of the oxidized dye with and without redox couple is shown. When redox couple is added the signal falls of faster than without the redox couple. By fitting the data by double or single exponential decay the time constant for the regeneration and recombination were calculated.

The efficiency of the regeneration can be calculated according to Equation 4.21.

$$\eta_{reg} = \frac{k_{reg}}{k_{reg} + k_{rec}} = 1 - \frac{t_{\frac{1}{2}redox}}{t_{\frac{1}{2}inert}} \tag{4.21}$$

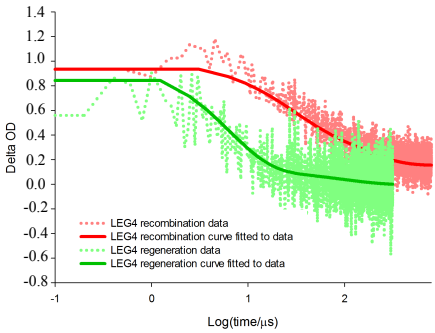

Figure 4.17. TAS measurements of the LEG4 dye with full electrolyte composition in acetonitrile and with only stock solution in acetonitrile (without redox couple).

Where k_{reg} and k_{rec} are the rate constants for the regeneration and recombination respectively. $t_{\frac{1}{2}redox}$ and $t_{\frac{1}{2}inert}$ are the half-times with and without redox mediator, giving the regeneration and recombination half-times.

4.2.6 Photoelectron spectroscopy

In this thesis photoelectron spectroscopy (PES) was used in paper II. For a more extensive description of PES and its application for DSC see elsewhere [61]. PES is a surface sensitive techniques that can give information about the chemical environment of different atoms. In short, the photoelectric effect is the basic principle behind PES. The sample under investigation is irradiated by X-ray photons. Depending on the energy of the radiation and the energy level in the atom, which an electron originate from, the emitted photoelectron will have different kinetic energy E_{kin}, as described in Equation 4.22.

$$E_{kin} = h\nu - \phi - E_{bin} \tag{4.22}$$

E_{bin} is the binding energy of the electron in the atom and ϕ is the work function. Since every element has very specific energy levels, it is possible to distinguish one element from another. In PES the numbers of emitted electrons are measured as a function of kinetic energy for a well defined photon energy. In Figure 4.18 an example of a PES spectrum is illustrated, in this spectrum the binding energy increase to the left meaning that the kinetic energy of the emitted photoelectrons increase to the right on the x-axis. The y-axis shows the intensity/number of electrons.

PES is a surface sensitive technique. The photons travel easily into a material without interacting with electrons. However, the electrons are sensitive for interaction with the positively charged cores or other electrons. The intensity

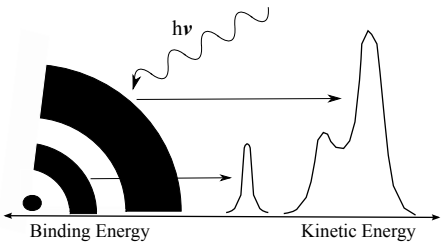

Figure 4.18. Illustration of an atom and its different energy levels and how they correspond to the binding energy and the kinetic energy in a X-ray PES spectrum.

of the photoejected electrons measured by the detector depends on several parameters, for a more comprehensive discussion see elsewhere [61].

4.2.7 Scanning electron microscopy

In this thesis scanning electron microscopy (SEM) was used for studying the surface of the PEDOT counter electrodes in paper II. SEM is a technique where an image of a sample is created by scanning it with a beam of electrons. The electron beam interact with the atoms on the surface of the sample giving information about surface topography and composition. The most common mode of detection is by secondary electrons emitted by atoms excited by the electron beam. In order to be able to measure SEM the sample needs to be electrically conductive, at least at the surface, and electrically grounded to prevent accumulation of electrostatic charge at the surface.

4.2.8 Matrix assisted laser desorption/ionizing mass spectroscopy

MALDI is a technique of ionizing the sample in a soft way which is often used in biochemistry for detection of aminoacids, DNA, peptides and proteins. The technique consists of mixing the sample with a matrix, most often a small organic molecule. The matrix and the sample crystallize on the sample holder, a conductive target. The first part of the measurement is that the sample gets irradiated by a UV-vis laser and ablation takes place. In the plume formed the analyte molecules charge (protonated or deprotonated). The mechanism of MALDI is still under debate. The charged analyte molecules travel to the detector and a spectrum of intensity versus mass through charge is created, as in other mass spectroscopy techniques. In this thesis MALDI-MS was used for investigating the complexation by the glycolic chains of the V35 dye with

cations in the electrolyte. More extensive description of the technique is found elsewhere [62].

5. Discussion of papers

This thesis is based on four papers. Down below follows a discussion of the results from the papers.

5.1 Paper I

PEDOT counter electrodes for dye-sensitized solar cells prepared by aqueous micellar electrodeposition

The PEDOT electrodes in paper I were fabricated by electropolymerizing the monomer 3,4-ethylenedioxythiophene (EDOT) see Figure 5.1 by applying constant current, galvanostatic mode.

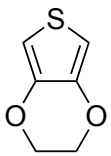

Figure 5.1. The monomer EDOT.

The polymer PEDOT is created by the monomer EDOT being reduced at the working electrode and forming a radical. The polymerization can continue by the radical reacting with another radical or a monomer creating a bimer radical. PEDOT is illustrated in Figure 5.2.

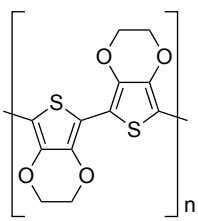

Figure 5.2. The conductive polymer PEDOT.

Electropolymerization of EDOT has earlier been performed in acetonitrile solution and in ionic liquids. However, water is an ideal solution for the process due to it being non-toxic and environmentally friendly. EDOT is unfortunately not water soluble. In this study EDOT was electropolymerized in water with addition of a surfactant, sodium dodecyl sulfate (SDS), forming micelles. The electropolymerization of EDOT was successfully performed on both flexible plastic substrates and on larger glass substrates (9×9 cm^2), giving PEDOT surfaces.

The electropolymerization was carried out under galvanostatic constant current conditions. A two electrode setup was used, a constant current of 13 mA/81cm^2 was applied and the working electrode potential was about 1.22 Volt versus NHE. By experiments it was found that the best homogeneity of the polymerization was found using constant current conditions (chronopotentiometry) compared to using constant potential conditions (chronoamperometry). By varying the time of deposition different thicknesses of the polymer (PEDOT) were obtained.

The resulting PEDOT glass substrates were used as counter electrodes in DSC:s with cobalt-based redox mediator. The solar cells assembled with PEDOT counter electrodes gave about 10 times lower R_{ce}, higher FF and higher η, compared to platinized counter electrodes. The PEDOT surfaces showed to have a higher surface area by SEM pictures and capacitance values. The SEM pictures indicate a cauliflower structure and the capacity is more than 100 times higher for the PEDOT compared to the platinized substrates. The higher capacitance values of the PEDOT samples could however also be explained by the redox activity of the PEDOT. The obtained R_{ce}:s were used in the linear approximation of the Butler-Volmer equation to calculate the exchange current densities. The PEDOT electrodes gave 100 mA cm^{-2} while the platinized electrodes gave 4.6 mA cm^{-2}. This indicates once again a higher catalytic performance of the PEDOT electrodes facilitating the reduction of the oxidized species in the electrolyte, compared to the platinized electrode.

In paper I the diffusion coefficients for the redox couple (cobalt) were investigated by three different methods. First by measuring the limiting current of two PEDOT counter electrodes sandwiched with electrolyte in between, see Figure 5.3 and using the relationship:

$$J_{lim} = \frac{2FDC_{Co(III)}}{\sigma} \tag{5.1}$$

where F is the Faraday constant, D is the diffusion coefficient of the oxidized species in the electrolyte ($Co(III)$), and σ is the spacing between the electrodes.

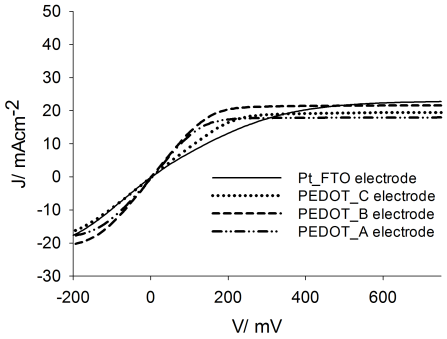

Figure 5.3. IV curve of cobalt electrolyte sandwiched between PEDOT or platinized electrodes. The different PEDOT electrodes have different times of electropolymerization of EDOT resulting in different thicknesses. The different electropolymerization times were: electrode A = 280 seconds, electrode B = 320 seconds and electrode C = 450 seconds. One electrode is also platinized for comparison.

The obtained value for $Co(bpy)_3^{3+}$ was $(6.2 \pm 0,6) \times 10^{-6} cm^2 s^{-1}$. This value has however relatively high error. This is probably due to the deviation in the spacing between the electrodes (σ), it could also be that the concentration of $Co(bpy)_3^{3+}$ change slightly when it is brought in contact with the PEDOT counter electrodes.

The diffusion coefficient was also calculated by Equation 4.13.

Equation 4.13 has earlier been used for obtaining the diffusion coefficients but in iodide/triiodide redox couple system [54]. It should be pointed out that the equation is for an ideal solution, meaning that the interactions between all species in the solution are the same. In a solar cells electrolyte containing different charged species, deviation from ideality will most probable occur. This is shown by Kloo and co-workers and also in paper I where the obtained value of the diffusion coefficient from Equation 4.13 ($2.3 \pm 0.2 \times 10^{-6} cm^2 s^{-1}$) deviate from both the values obtained by limiting current of two PEDOT electrodes sandwiched and measured by IV ($6.2 \pm 0.6 \times 10^{-6} cm^2 s^{-1}$) and the microelectrode limiting current measurements ($4.3 \times 10^{-6} cm^2 s^{-1}$ for Co(III) and $4.6 \times 10^{-6} cm^2 s^{-1}$ for Co(II)).

5.2 Paper II

Linker unit modification of triphenylamine-based organic dyes for efficient cobalt mediated dye-sensitized solar cells

The organic donor-linker-acceptor dye D35 has earlier been shown to be efficient in cobalt-based mediator DSC:s. Since D35 only harvest photons below 620 nm a red shift is needed in order to obtain higher power conversion efficiencies. In this study a series of dyes, the LEG-series (LEG1, LEG2, LEG3 and LEG4) see Figure 5.4, based on the D35 dye was synthesized.

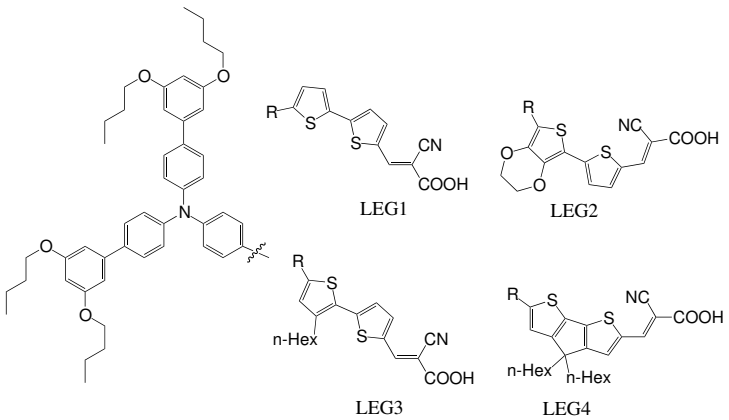

Figure 5.4. The LEG-series of dyes.

The absorption spectra were red shifted by modifying the π conjugated linker unit. Even though all LEG-dyes had broader absorption spectrum, only two outperformed D35 (LEG3 and LEG4) when evaluating the power conversion efficiencies. The reason for this was investigated by addition of co-absorber (CDCA), electron lifetime measurements, TAS-measurements and PES-measurements. CDCA has earlier been used in studies to avoid dye aggregation [63]. By comparing IPCE spectra, V_{oc}:s, and J_{sc}:s of solar cells assembled without and with CDCA the results indicate that aggregation could be a problem for LEG2. It is seen in Figure 5.5b compared to Figure 5.5a how the addition of CDCA increase the IPCE for LEG2. The lower IPCE values for LEG1 and LEG2 could be due to aggregation since monomers inject better than aggregates [64]. However, only LEG2 has increased power conversion efficiency upon addition of CDCA.

The LEG4 and LEG2 dyes obtained relatively low V_{oc}:s values compared to the D35 dye and the other LEG-dyes. This was investigated by measuring the electron lifetimes. The V_{oc} is the difference between *quasi*-Fermi level and the redox level of the redox couple in the electrolyte. Since all solar cells were assembled with the same electrolyte, the *quasi*-Fermi of the photoelectrode

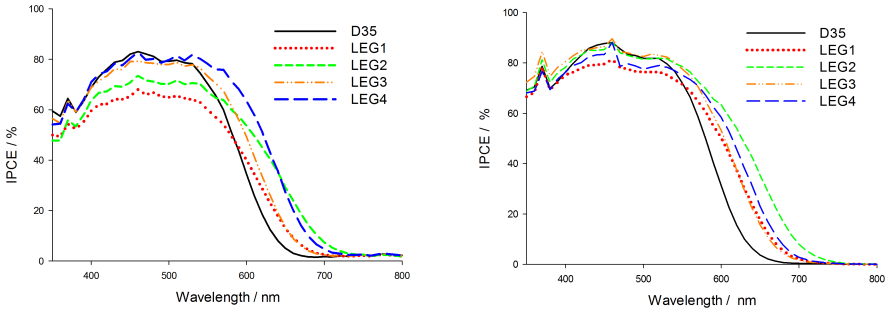

Figure 5.5. IPCE of the LEG-series of dyes without (a) and with (b) CDCA.

determined the V_{oc}. The *quasi*-Fermi level is limited by the conduction band edge, by measuring extracted charge see Figure 5.6 it could be concluded that the sensitizes did not significantly change the conduction band. This leading to that the differences in electron lifetime governs the V_{oc}:s.

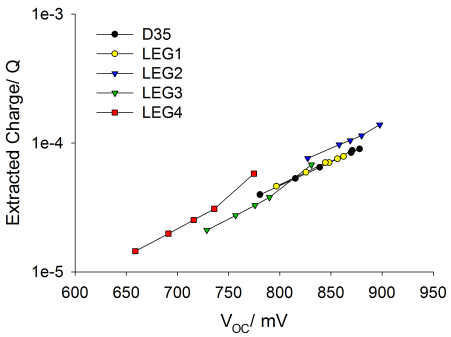

Figure 5.6. Extracted charge measurements of the LEG-series of dyes.

When CDCA was added the electron lifetimes increased for LEG2 in agreement with the increased V_{oc}. In Figure 5.7a and Figure 5.7b it can be seen how all LEG-dyes improved their electron lifetimes when adding CDCA as co-adsorber, compared to D35. The performance of D35 has earlier been shown not to improve when adding CDCA [65].

Transient nanosecond laser measurements were used to evaluate regeneration and recombination of the LEG-series. It was found that LEG2 and LEG1 attained low regeneration efficiencies due to for LEG2 slow regeneration and for LEG1 fast recombination. The slow regeneration for LEG2 could be an indication of aggregation.

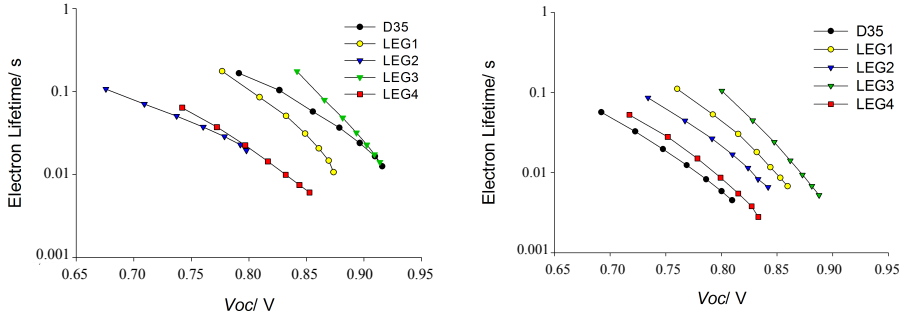

Figure 5.7. Electron lifetimes of the LEG-series of dyes without (a) and with (b) CDCA.

PES was utilized for deriving the binding angles of the LEG-series of dyes on the TiO_2 surface and the surface coverage. The intensity of the measured photoejected electrons depend on several parameters. One of them is the average distance the electrons travel without energy loss, this is called the inelastic mean free path (IMFP). Equation 5.2 shows how the intensity I, is related to the IMFP λ, the intensity of the background I_0 and the distance between two atoms, d. The equation is valid for a flat surface.

$$\frac{I}{I_0} = e^{-\lambda d} \tag{5.2}$$

In paper II Equation 5.2 was used for calculating the distance between two atoms in the dye molecules. The dyes in the LEG-series contain two different nitrogens, one in the donor unit (N_D), the triphenylamine unit, and one in the acceptor unit, the cyanoacrylic acid (N_A). Intensities of two different photon energies were measured, IMFP was taken as 6 Å and 8 Å for the two photon energies [66, 67], by solving the system of equations, Equation 5.2 gave d as the distance between the two nitrogens. Trigonometry was used to calculate the binding angles of the dyes, see Figure 5.8.

By this estimation it was found that LEG4 has the greatest angle to the TiO_2 normal and LEG1 the smallest, meaning that LEG1 is "standing up" the most. LEG2 and LEG3 have similar bingding angles.

Since all LEG-dyes and the D35 dye contain sulfur, and the sulfur atom is positioned close to the TiO_2 surface with small difference in distance, this makes it suitable for comparing dye coverage. The S 2p core level spectra were measured, see Figure 5.9, and the intensities were normalized with respect to LEG4, this gave a comparison of the surface coverages and LEG4 was shown to have the lowest surface coverage. The surface coverage was also calculated by desorption measurements giving the same results. The low surface cover-

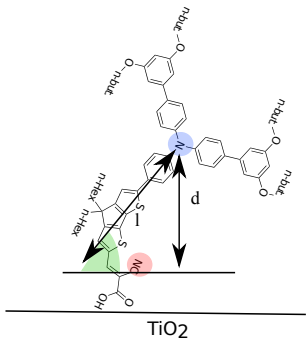

Figure 5.8. Illustration of how the binding angles were estimated. Green area indicates the angle. The blue circle marks the donor nitrogen while the red the acceptor nitrogen. *d* is the distance calculated by PES-measurements, *l* is the length calculated by estimation of bond lengths.

age and the large binding angle to the TiO_2 normal for LEG4 dye explain the low V_{oc}.

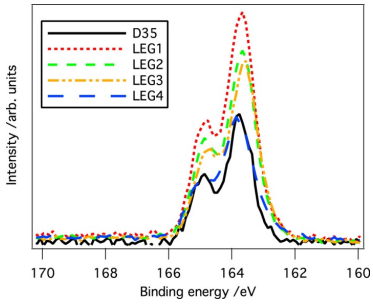

Figure 5.9. PES spectra of the S2p core level photoelectrons of the LEG-dyes. The intensities were used to calculate the surface coverage.

Paper II shows that it was not enough to red shift the spectral response of dyes for obtaining higher power conversion efficiencies. By changing the architecture of the dyes the binding morphology was effected, having implications on the performances of the solar cells. The LEG4 dye gave the highest power conversion efficiencies mainly attributed to the red-shift and higher molar extinction coefficient. But LEG4 showed low V_{oc} and low surface coverage, probably due to the hexane chains in the linker unit resulting in less dense packing.

5.3 Paper III

Organic hydrophilic dye for water-based dye-sensitized solar cells

As already stated in paper I, water would be an ideal solvent for fabrication of DSC:s since it is non-toxic and environmentally friendly. In 2010, 2012 and 2013 some papers were published were water was investigated as solvent for the electrolyte in the DSC [47, 49, 48, 50, 32]. These papers inspired to the study of paper III. Some of these papers employed hydrophobic dyes in order to avoid desorption [47, 49]. Surfactants were also utilized, in order to increase the wetting of the water-based electrolyte in the mesoporous sensitized TiO_2 structure, or to dissolve the water insolvable additives such as TBP [47, 49, 32, 50]. In paper III a hydrophilic dye, V35, was synthesized and investigated. The dye is a modification of the organic donor-linker-acceptor dye D35. The n-butoxy chains on the triphenylamine unit were substituted for glycolic chains, increasing the wettability of the sensitized TiO_2 surface in contact with both pure water and electrolyte remarkably. The dye did not desorb in water. The increased wettability by the glycolic chains was shown by contact angles measured both with pure water and electrolytes. PIA measurements showed that the regeneration of the hydrophilic V35 dye was more complete, than for the hydrophobic D35 dye, in water-based electrolytes.

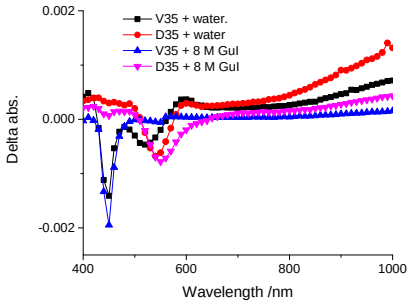

Figure 5.10. PIA spectra of V35 and D35 with water-based electrolyte. V35 is fully regenerated compared to D35, which still shows positive absorption signal above 800 nm.

In Figure 5.10 it can be seen how the measurements carried out without redox couple give strong positive signals in the region above 800 nm, being absorbance of the oxidized dyes. When redox couple is added in the electrolytes, the positive signal disappears for the V35 dye, implying regeneration. D35, however, still shows positive signal in the region above 800 nm. It should also be noted that around 900 nm injected electrons in the TiO_2 are absorbing. However, the conclusion of the experiment is the same.

Different compositions of electrolytes were investigated utilizing salts like KI, NaI and I_2. Since it had been reported earlier that guanidinium salts and CDCA effect water-based DSC positively [49] this was investigated in the V35 system. Guanidinium iodide was used instead of earlier tested NaI and KI. While the difference in performance for V35 and D35 had been relatively large with the KI and NaI salts (for example 2.2% versus 0.3%) the difference in performance with the guanidinium salt showed not the same difference (1.97% versus 1.95%).

When adding the co-absorber CDCA the electron lifetime and V_{oc} increased for the V35 dye. This could indicate aggregation (as for LEG2 in Paper II) or greater binding angle versus the TiO_2 normal (as for LEG4) for the V35 dye. CDCA has in other studies been shown to prevent dye aggregation [63]. It has been shown earlier that CDCA does not shift the conduction band [68]. Since the conduction band does not shift, the *quasi*-Fermi levels of the solar cells assembled with and without CDCA should be the same. Since the solar cells are assembled with the same electrolyte the redox level of the redox mediator is the same. The explanation for the increased electron lifetime and V_{oc} upon addition of CDCA in the V35 system could be; the glycolic chains of the V35 dye cause aggregation. CDCA prevent this, by splitting up the aggregates. The glycolic chains interact with the positive charges on the TiO_2 surface and thereby have an increased binding angle versus the TiO_2 normal. The increased angle versus the normal cause a decreased recombination path for the electrons in the conduction band to the positively charge on the oxidized dye situated on the triphenylamin unit [69, 70]. This may cause increased recombination and decreased V_{oc}. Adding CDCA could prevent this by "tilting" up the V35 dyes from the surface and "screening" the TiO_2 from the redox mediator.

Different pH values in the electrolyte were also tested (pH 8 and pH 9), the results showed very similar. The higher pH gave higher V_{oc} but lower current while the lower pH the opposite. The combination of CDCA and pH 8 and pH 9 in the electrolyte did not give any increased performance since CDCA probably desorbs from the TiO_2 surface at basic conditions. This paper showed that a hydrophilic dye in combination with water-based electrolytes based on simple salts, increased the wettability, current and power conversion efficiency compared to a hydrophobic dye.

5.4 Paper IV

Laser desorption/ionization mass spectrometry of dye-sensitized solar cells: identification of the dye-electrolyte interaction

In this paper MALDI MS was employed to investigate further the interactions between the hydrophilic dye, V35, and the electrolytes used in paper III. Since DSC:s are fabricated on conductive glass they can be investigated by MALDI MS without further pre-treatment. A holder for the DSC:s was fabricated, DSC:s were opened and mounted into the apparatus directly. The results show that the glycolic chains of V35 form complexes with the Na^+ and the K^+ but not with the guanidinium ions. The D35 samples did not show any complexation with any cation. These results indicate that the better performance in the V35 dye water-based electrolyte system could be partly due to the complex of the glycolic chains with the cations. This facilitate the attraction of the negatively charged I_3^- that regenerates the dye. The regeneration process is simply facilitated by the glycolic chains on the V35 dye compared to the n-buthoxy chains on the D35 dye.

6. Acknowledgments

I would like to thank my supervisors Anders Hagfeldt, Gerrit Boschloo and Erik Johansson for accepting me as a Ph.D student, helping me and for the great working environment.

I would like to thank Nick Vlachopoulos for help with electrochemistry and general scientific questions. I would like to thank the French collaborators Christian Perruchot and Mohamed Jouini for all the help and support with my first article.

Old members, new members and current members of the Hagfeldt group for collaborations and scientific discussions. Among the old members especially Peter Lohse and Sandra Feldt for the nice work with paper number II. Susanna, thanks for all the PES-work, discussions and help in general.

At KTH I would like to thank Erik Gabrielsson, Martin Karlsson and Qian Gao for all chemicals and necessary material for dye-sensitized solar cells.

I would like to thanks Denys Shevchenko at BMC for the nice collaboration.

Thanks to Anna Eriksson, Malin Johansson, Nick Vlachopoulos and Wenxing Yang for helping me proofreading this thesis. Anna should have a special thank you for helping me with my first teaching, my first semester as a Ph.D student.

Julia Liljestrand for always being willing to help with the school solar cells. At TEKNAT samverkan I would like to thank Sami Vihriälä and Tobias Blom for giving me the possibility to do Levande frågelådan/SciFest/Visiting days /Lärarlyftet/school visits et cetrera. Meeting some of all these people makes one believe in humankind and the future!

Last but not least all the other people at Ångström providing me with joy, inspiration, motivation, knowledge and help, especially Mohammad Mirmohades, Sonja Pullen, Djawed Nauroozi and Katharina Brinkert.

References

[1] REN21. Renewables 2013 global status report. Technical report, REN21, 2013.

[2] IPCC. Climate change 2013 the physical science basis. Technical report, IPCC, 2013.

[3] N. S. Lewis. Toward cost-effective solar energy use. *Science*, 315(5813):798–801, 2007.

[4] NREL. Best research-cell efficiencies, August 2014.

[5] N. K. Noel.; S. D. Samuel.; A. Abate.; C. Wehrenfennig.; S. Guarnera.; A. Haghighirad.; A. Sadhanala.; G. E. Eperon.; S. K. Pathak.; M. B. Johnston.; A. Petrozza.; L. M. Herza.; H. J. Snaith. Lead-free organic-inorganic tin halide perovskites for photovoltaic applications. *Energy and Environmental Science*, 7:3061–3068, 2014.

[6] H. J. Queisser W. Shockley. Detailed balance limit of efficiency of pn junction solar cells. *Journal of Applied Physics*, 32(3):510–519, 1961.

[7] R. Memming. Electron transfer process with excited molecules at semiconductor electrodes. *Progress in Surface Science*, 17:7–74, 1984.

[8] H. Tsubomura.; M. Matsummura.; Y. Nomura.; T. Amamiya. Dye sensitized zinc oxide: aqueous electorlyte: platinum photocell. *Nature*, 261, 1976.

[9] J. Desilvestro.; M. Grätzel.; L. Kavan.; J. Moser. Highly efficient sensitization of titanium dioxide. *Journal of American Chemical Society*, 107:2988–2990, 1985.

[10] B. O'Regan.; M. Grätzel. A low cost, high-efficiency solar cell based on dye-sensitized collodial tio2 films. *Nature*, 353:737–739, 1991.

[11] U. Bach.; D. Lupo.; P. Comte.; J. E. Moser.; F. Weissortel.; J. Salbeck.; H. Spreitzer.; M. Grätzel. Solid state dye sensitized mesoporous tio2 solar cells with high photon to electron conversion efficiencies. *Nature*, 395:583–585, 1998.

[12] Prashant V. Kamat. Boosting the efficiency of quantum dot sensitized solar cells through modulation of interfacial charge transfer. *Accounts of Chemical Research*, 45(11):1906–1915, 2012.

[13] I. J. Kramer.; E. H. Sargent. The architecture of colloidal quantum dot solar cells materials to the architecture of colloidal quantum dot solar cells: Materials to the architecture of collodial quantum dot solar cells materials to devices. *Chemical Reviews*, 114:863–882, 2014.

[14] X. L. Zhang.; F. Huang.; A. Nattestad.; K. Wang.; D. Fu.; A. Mishra.; P. Baurle.; U. Bach.; Y. B. Cheng. Enhanced open circuit voltage of p-type dsc with highly crystalline nio nanoparticles. *Chemical Communitcations*, 47:4808–4810, 2011.

[15] A. Kojima.; K. Teshima.; Y. Shirai.; T.; Miyasaka. Organometal halide perovskites as visible light sensitizers for photovoltaic cells. *Journal of American Chemical Society*, 131:6050–6051, 2009.

[16] M. M. Lee.; J. Teuscher.; T. Miyasaka.; T. N. Murakami.; H. J. Snaith. Efficient hybrid solar cells based on meso superstructured organometal halide perovskites. *Science*, 338:643–647, 2012.

[17] H.-S. Kim.; C.-R. Lee.; J.-H. Im.; K-B Lee.; T. Moehl.; A. Marchioro.; S.-J. Moon.; R. Humphry-Baker.; J.-H. Yum.; J. E. Moser.; M. Grätzel.; N.-G. Park. Lead iodide perovskite sensitized all-solid-state submicron thin film mesoscopic solar cell with efficiency exceeding 9%. *Scientific reports*, 2:591, 2012.

[18] J. Burschka.; N. Pellet.; S. J. Moon.; R. Humphry-Baker.; P. Gao.; M. K. Nazeeruddin.; and M. Grätzel. Sequential deposition as a route to high performance perovskite sensitized solar cells. *Nature*, 499:316–319, 2013.

[19] B. Li.; L. Wang.; B. Kang.; P. Wang.; Y. Qiu. Review of recent progress in solid state dye sensitized solar cells. *Solar Energy Materials and Solar Cells*, 90:549–573, 2006.

[20] K. Hanabusa.; D. Inoue.; M. Suzuki.; M. Kimura.; H. Shirai. Physical gelation of organic solvents by low molecular weight gelators and preparation of organogel electrolytes. *Polymer Journal*, 31:1159–1164, 1999.

[21] Ze Yu. *Liquid Redox Electrolytes for Dye sensitized Solar Cells*. PhD thesis, Royal Institute of Technology, 2012.

[22] J. Zhang.; L. Häggman.; M. Jouini.; A. Jarboui.; G. Boschloo.; N. Vlachopoulos.; A. Hagfeldt. Solid-state dye sensitized solar cells based on poly(3,4 ethylenedioxypyrrole) and metal free organic dyes. *Chem Phys Chem Communications*, 15:1043–1047, 2014.

[23] J. Zhang.; L Yang.; Y. Shen.; B. W. Park.; Y. Hao.; E. M. J. J.; G. Boschloo.; L. Kloo.; E. Gabrielsson.; L. Sun.; A. Jarboui.; C. Perruchot.; M. Jouini.; N. Vlachopoulos.; A. Hagfeldt. Poly (3,4 ethylenedioxythiophene) hole transporting material generated by photoelectrochemical polymerization in aqueous and organic medium for all solid state dye sensitized solar cells. *The Journal of Physical Chemistry C*, 118(30):16591–16601, Michael Grätzel Festschrift 2014.

[24] S. Ardo.; G. J. Meyer. Photodriven heterogeneous charge transfer with transition metal compounds anchored to tio2 semiconductor surfaces. *Chemical Society Reviews*, 38:115–164, 2009.

[25] S. M. Feldt.; P. W. Lohse.; F. Kessler.; M. K. Nazeeruddin.; M. Grätzel.; G. Boschloo.; A. Hagfeldt. Regeneration and recombination kinetics in cobalt polypyridine based dye sensitized solar cells, explained using marcus theory. *Physical Chemistry Chemical Physics*, 15:7087–7097, 2013.

[26] J. Bisquert.; A. Zaban. The trap limited diffusivity of electrons in nanoporous semiconductor networks permeated with a conductive phase. *Applied Physics A*, 77:507–514, 2003.

[27] M. Grätzel. Photoelectrochemical cells. *Nature*, 414:338–344, 2001.

[28] A. Fujishima.; K. Honda. Electrotechnical photolysis of water at a semiconductor electrode. *Nature*, 238:37–38, 1972.

[29] A. Hagfeldt.; G. Boschloo.; L. Sun.; L. Kloo.; H. Pettersson. Dye sensitized solar cells. *Chemical Reviews*, 110(11):6595–6663, 2010.

[30] K. Hauffe.; H. J. Danzmann.; H. Pusch.; J. Range.; H. Volz. New experiments on the sensitization of zinc oxide by means of the electrochemical cell technique. *Journal of Electrochemical Society*, 117(8):993–999, 1970.

[31] S. Ahmad.; T. Bessho.; F. Kessler.; E. Baranoff.; J. Frey.; C. Yi.; M. Grätzel.; M. K. Nazeeruddin. A new generation of platinum and iodine free efficient dye sensitized solar cells. *Physical Chemistry Chemical Physics*, 14:10631–10639, 2012.

[32] H. Tian.; E. Gabrielsson.; P. W. Lohse.; N. Vlachopoulos.; L. Kloo.; A. Hagfeldt.; L. Sun. Development of an organic redox couple and organic dyes for aqueous dye sensitized solar cells. *Energy and Enviromental Science*, 5:9752–9755, 2012.

[33] J. D. Roy Mayhew.; G. Boschloo.; A. Hagfeldt.; I. A. Aksay. Functionalized graphene sheets as a versatile replacement for platinum in dye sensitized solar cells. *Applied Material Interfaces*, 4:2794–2800, 2012.

[34] Md. K. Nazeeruddin.; S. M. Zakeeruddin.; R. Humphry-Baker.; M. Jirousek.; P. Liska.; N. Vlachopoulos.; V. Shklover.; C. H. Fischer.; M. Grätzel. Acid-base equilibria of (2, 2'-bipyridyl-4, 4'-dicarboxylic acid) ruthenium (ii) complexes and the effect of protonation on charge-transfer sensitization of nanocrystalline titania. *Inorganic Chemistry*, 38(26):6298–6305, 1999.

[35] L. Cevey.; E. Costa.; V. Shklover.; L. Spiccia.; B. G. Deacon.; C. A. Bignozzi.; M. Grätzel P. Pechy.; T. Renouard.; S. M. Zakeeruddin.; R. Humphry-Baker.; P. Comte.; P. Liska. Engineering of efficient panchromatic sensitizers for nanocrystalline tio2-based solar cells. *Journal of the American Chemical Society*, 123(8):1613–1624, 2001.

[36] G. Boschloo.; A. Hagfeldt. Characteristics of the iodide/triiodide redox mediator in dye-sensitized solar cells. *Accounts of Chemical Research*, 42(11):1819–1826, 2009.

[37] S. Mathew.; A. Yella.; P. Gao.; R. Humphry-Baker.; B. F. E. Curchod.; N. Ashari-Astani.; I. Tavernelli.; U. Rothlisberger.; M K. Nazeeruddin.; M. Grätzel. Dye sensitized solar cells with 13 percent efficiency achieved through the molecular engineering of porphyrin sensitizers. *Nature Chemistry*, 6(242-247), 2014.

[38] S. M. Feldt.; E. A. Gibson.; E. Gabrielsson.; L. Sun.; G. Boschloo.; A. Hagfeldt. Design of organic dyes and cobalt polypyridine redox mediators for high efficiency dye sensitized solar cells. *Journal of American Chemical Society*, 132:16714–16724, 2010.

[39] G. Boschloo.; E. A. Gibson.; A. Hagfeldt. Photomodulated voltammetry of iodide/triiodide redox electrolytes and its relevance to dye sensitized solar cells. *The Journal of Physical Chemistry C*, 2:3016–3020, 2011.

[40] P. Liska.; N. Vlachopoulos.; M. K. Nazeeruddin.; P. Comte.; M. Grätzel. cis -diaquabis(2,2'-bipyridyl4,4'-dicarboxylate)- ruthenium(ii) sensitizes wide band gap oxide semiconductors very efficiently over a broad spectral range in the visible. *Journal of American Chemical Society*, 110:3686–3687, 1988.

[41] N. Vlachopoulos.; P. Liska.; J. Augustynski.; M. Grätzel. Very efficient visible light energy harvesting and conversion by spectral sensitization of high surface area polycrystalline titanium dioxide films. *Journal of American Chemical Society*, 110:1216–1220, 1988.

[42] A. Hagfeldt. *Microporous and polycrystalline semiconductors electrodes studied by photoelectrochemical methods supported by quantum chemical calculations and photoelectron spectroscopy*. PhD thesis, Uppsala University,

1993.

[43] B. Macht.; M. Turrion.; A. Barkschat.; P. Salvador.; K. Ellmer.; H. Tributsch. Patterns of efficiency and degradation in dye sensitization solar cells measured with imaging techniques. *Solar Energy Materials and Solar Cells*, 73:163–173, 2002.

[44] Y. Liu.; A. Hagfeldt.; X. R. Xiao.; S. E. Lindquist. Investigation of influence of redox species on the interfacial energetics of a dye sensitized nanoporous tio2 solar cell. *Solar Energy Materials and Solar Cells*, 55:267–281, 1998.

[45] M. Sumita.; K. Sodeyama.; L. Han.; Y. Tateyama. Water contamination effect on liquid acetonitrile/tio2 anatase (101) interface for durable dye-sensitized solar cell. *The Journal of Physical Chemistry C*, 115:19849–19855, 2011.

[46] Y. S. Jung.; B. Yoo.; M. K. Lim.; S. Y. Lee.; K. J. Kim. Effect of triton x 100 in water added electrolytes on the performance of dye sensitized solar cells. *Electrochimica Acta*, 54:6286–6291, 2009.

[47] C. Law.; S. C. Pathirana.; X. Li.; A. Y. Anderson.; P. R. F. Barnes.; A. Listorti.; T. H. Ghaddar.; B. C. O'Regan. Water based electrolytes for dye sensitized solar cells. *Advansed Materials*, 22:4505–4509, 2010.

[48] T. Daeneke.; Y. Uemura.; N. W. Duffy.; A. J. Mozer.; N. Koumura.; U. Bach.; L. Spiccia. Aqueous dye sensitized solar cell electrolytes based on the ferricyanide ferrocyanide redox couple. *Advanced Materials*, 24:1222–1225, 2012.

[49] C. Law.; O. Moudam.; S. Villarroy Lidon.; B. O'Regan. Managing wetting behavior and collection efficiency in photoelectrochemical devices based on water electrolytes improvement in efficiency of water/iodide dye sensitised cells to 4%. *Journal of Materials Chemistry*, 22:2387–2394, 2012.

[50] W. Xiang.; F. Huang.; Y. B. Cheng.; U. Bach.; L. Spiccia. Aqueous dye sensitized solar cell electrolytes based on the cobalt(ii)/(iii) tris(bipyridine) redox couple. *Energy and Environmental Science*, 6:121–127, 2013.

[51] C. E. Richards.; A. Y. Anderson.; S. Martiniani.; C. Law.; B. C. O'Regan. The mechanism of iodine reduction by tio2 electrons and the kinetics of recombination in dye-sensitized solar cells. *Journal of Physical Chemsitry Letters*, 3:1980–1984, 2012.

[52] G. Boschloo.; L. Häggman.; A. Hagfeldt. Quantification of the effect of 4-tert-butylpyridine addition to i-/i3- redox electrolytes in dye-sensitized nanostructured tio2 solar cells. *Journal of Physical Chemistry B*, 110:13144–13150, 2006.

[53] Jarl Nissfolk. *Charge Transport Processes in Mesoporous Photoelectrochemical Systems*. PhD thesis, Royal Institute of Technology, 2009.

[54] Z. Yu.; M. Gorlov.; J. Nissfolk.; G. Boschloo.; L. Kloo. Investigation of iodine concentration effects in electrolytes for dye-sensitized solar cells. *The Journal of Physical Chemistry C*, 114:10612–10620, 2010.

[55] F. Fabregat-Santiago.; J. Bisquert.; G. Garcia-Belmonte.; G. Boschloo.; A. Hagfeldt. Influence of electrolyte in transport and recombination in dye-sensitized solar cells studied by impedance spectroscopy. *Solar Energy Materials and Solar Cells*, 87:117–131, 2005.

[56] M. Wang.; P. Chen.; R. Humphry-Baker.; S. M. Zakeeruddin.; M. Grätzel. The influence of charge transport and recombination on the performance of dye-sensitized solar cells. *ChemPhysChem*, 10(1):290–299, 2009.

[57] A. J. Bard.; L. R. Faulkner. *Electrochemical Methods: Fundamentals and Applications*. John Wiley and Sons, Inc, 2001.
[58] V. V. Pavlishchuk.; A. W. Addison. Conversion constants for redox potentials measured versus different reference electrodes in acetonitrile solutions at 25°c. *Inorganica Chimica Acta*, 298:97–102, 2000.
[59] G. Boschloo.; A. Hagfeldt. Photoinduced absorption spectroscopy as a tool in the study of dye-sensitized solar cells. *Inorganica Chimica Acta*, 361:729–734, 2008.
[60] U. Cappel. *Characterisation of Organic Dyes for Solid State Dye-Sensitized Solar Cells*. PhD thesis, Uppsala University, 2011.
[61] Rebecka Lindblad. *Electronic Structure and Energy Level Alingnment in Mesoscopic Solar Cells*. PhD thesis, Uppsala University, 2014.
[62] N. Bergman.; D. Shevchenko.; J. Bergquist. Approaches for the analysis of low molecular weight compounds with laser desorption/ionization techniques and mass spectrometry. *Analytical Bioanalytical Chemistry*, 406:49–61, 2014.
[63] Z. S. Wang.; Y. Cui.; Y. Dan oh.; C. Kasada.; A. Shinpo.; K. Hara. Thiophene functionalized coumarin dye for efficient dye sensitized solar cells: Electron lifetime improved by coadsorption of deoxycholic acid. *The Journal of Physical Chemistry C*, 111:7224–7230, 2007.
[64] A. C. Khazraji.; S. Hotchandani.; S. Das.; P. V. Kamat. Controlling dye (merocyanine-540) aggregation on nanostructured tio2 films. an organized assembly approach for enhancing the efficiency of photosensitization. *Journal of Physical Chemistry B*, 103:4693–4700, 1999.
[65] X. Jiang.; T. Marinado.; E. Gabrielsson.; D. P. Hagberg.; L. Sun.; A. Hagfeldt. Structural modification of organic dyes for efficient coadsorbent-free dye-sensitized solar cells. *The Journal of Physical Chemistry C*, 114(6):2799–2805, 2010.
[66] M. Hahlin.; E. M. J. Johansson.; S. Plogmaker.; M. Odelius.; D. P. Hagberg.; L. Sun.; H. Siegbahn.; H. Rensmo. Electronic and molecular structures of organic dye/tio2 interfaces for solar cell applications: a core level photoelectron spectroscopy study. *Physical Chemistry Chemical Physics*, 12:1507–1517, 2010.
[67] Peter J Cumpson. Estimation of inelastic mean free paths for polymers and other organic materials: use of quantitative structure–property relationships. *Surface and interface analysis*, 31(1):23–34, 2001.
[68] T. Marinado.; M. Hahlin.; X. Jiang.; M. Quintana.; E. M. J. Johansson.; E. Gabrielsson.; S. Plogmaker.; D. Hagberg.; G. Boschloo.; S. M. Zakeeruddin.; M. Grätzel.; H. Siegbahn.; L. Sun.; A. Hagfeldt.; H. Rensmo. Surface molecular quantification and photoelectrochemical characterization of mixed organic dye and coadsorbent layers on tio2 for dye-sensitized solar cells. *The Journal of Physical Chemistry C*, 114:11903–11910, 2010.
[69] K. Westermark.; S. Tingry.; P. Persson.; H. Rensmo.; S. Lunell.; A. Hagfeldt.; H. Siegbahn. Triarylamine on nanocrystalline tio2 studied in its reduced and oxidized state by photoelectron spectroscopy. *The Journal of Physical Chemistry B*, 105:7182–7187, 2001.
[70] J. Nyhlen.; G. Boschloo.; A. Hagfeldt.; L. Kloo.; T. Privalov. Regeneration of oxidized organic photo-sensitizers in grätzel solar cells quantum chemical

portrait of a general mechanism. *Chem. phys. chem*, 11:1858–1862, 2010.
[71] R Vogel, P Hoyer, and H Weller. Quantum-sized pbs, cds, ag2s, sb2s3, and bi2s3 particles as sensitizers for various nanoporous wide-bandgap semiconductors. *The Journal of Physical Chemistry*, 98(12):3183–3188, 1994.
[72] C. Shi.; S. Dai.; K. Wang.; X. Pan.; F. Kong.; L. Hu. The adsorption of 4-tert-butylpyridine on the nanocrystalline tio2 and raman spectra of dye-sensitized solar cells in situ. *Vibrational Spectroscopy*, 39:99–105, 2005.
[73] M. K. Nazeeruddin.; A. Kay.; I. Rodicio.; R. Humpbry-Baker.; E. Muller.; P. Liska.; N. Vlachopoulos.; M. Grätzel. Conversion of light to electricity by cis-xzbis(2,2'-bipyridyl-4,4'-dicarboxylate)ruthenium(11) charge-transfer sensitizers (x = c1-, br-, i-, cn-, and scn-) on nanocrystalline tio2 electrodes. *Journal of American Chemical Society*, 115:6382–6390, 1993.
[74] A. Fujishima.; K. Kohayakawa.; K. Honda. Hydrogen production under sunlight with an electrochemical photocell. *Journal of Electrochemical Society*, 122(11):1487–1489, 1975.